

$L_{2,1}$ -Norm Regularized Quaternion Matrix Completion Using Sparse Representation and Quaternion QR Decomposition

Juan Han^a, Kit Ian Kou^{a,*}, Jifei Miao^b, Lizhi Liu^c, Haojiang Li^c

^aDepartment of Mathematics, Faculty of Science and Technology, University of Macau, Macau, 999078, China

^bSchool of Mathematics and Statistics, Yunnan University, Kunming, Yunnan, 650091, China

^cState Key Laboratory of Oncology in South China, Sun Yat-sen University Cancer Center, Guangzhou, Guangdong, 510060, China.

Abstract

Color image completion is a challenging problem in computer vision, but recent research has shown that quaternion representations of color images perform well in many areas. These representations consider the entire color image and effectively utilize coupling information between the three color channels. Consequently, low-rank quaternion matrix completion (LRQMC) algorithms have gained significant attention. We propose a method based on quaternion QR decomposition (QQR) and quaternion $L_{2,1}$ -norm called QLNLM-QQR. This new approach reduces computational complexity by avoiding the need to calculate the QSVD of large quaternion matrices. We also present two improvements to the QLNLM-QQR method: an enhanced version called IRQLNM-QQR that uses iteratively reweighted quaternion $L_{2,1}$ -norm minimization and a method called QLNLM-QQR-SR that integrates sparse regularization. Our experiments on natural color images and color medical images show that IRQLNM-QQR outperforms QLNLM-QQR and that the proposed QLNLM-QQR-SR method is superior to several state-of-the-art methods.

Keywords: Quaternion matrix completion, iteratively reweighted quaternion $L_{2,1}$ -norm, quaternion QR decomposition, low rank, sparse regularization

1. Introduction

Image completion, which endeavors to restore missing pixel values in an image from limited available data, has a broad spectrum of applications in computer vision and has garnered considerable research attention in recent years [1, 2, 3, 4]. Of all the techniques for completing images, those based on low-rank matrix completion (LRMC) have attained significant success. The majority of LRMC-based models fall into matrix rank minimization. As for matrix rank minimization, the low-rank property of matrices is used by LRMC-based models to primarily formulate a problem for minimizing matrices with low rank. Hence, the problem is usually converted into solving a constrained rank optimization problem by using the rank function.

*Corresponding author.

Email address: kikou@umac.mo (Kit Ian Kou)

Despite its effectiveness, the rank function poses a challenge due to its discontinuity and non-convexity, rendering it NP-hard. However, the nuclear norm has been demonstrated to be the most rigorous convex relaxation of the rank minimization problem [5]. Consequently, the nuclear norm, serving as a convex surrogate of the rank function, has been extensively employed to tackle image completion predicaments. Even so, the prevailing nuclear norm (NN) minimization methods, as noted by the authors in [6], tend to minimize all singular values simultaneously, leading to inadequate rank approximations. To remedy this, they proposed the truncated nuclear norm (TNN) regularization, which furnishes a more precise approximation of the rank function than the nuclear norm. Other comparable alternatives to TNN include the weighted nuclear norm (WNNM) [7, 2], the weighted Schatten p -norm [8], and the log-determinant penalty [9]. These methods also focus on optimizing the rank approximation, which entails processing the complete singular value decomposition (SVD). However, this can be computationally expensive and presents limitations for high-dimensional or big data applications. When it comes to matrix factorization, the general approach is to break down the original, larger matrix into at least two smaller matrices, often resulting in quicker numerical optimization [10, 11]. However, this factorization method can become enmeshed in local minima.

Besides, in the processing of color images using the aforementioned LRMC-based models, the RGB's three color channels are typically processed separately and then combined to obtain the final restoration outcome. However, this approach can result in a loss of coupling information between the three channels due to the disregard of the inter-channel relationships. Models that can more effectively use the connection between three channels are thus worth researching.

In recent years, the use of quaternion representation for color images has received significant attention from researchers. Various studies have demonstrated that quaternions can effectively describe color images, and approaches built upon quaternion representation have demonstrated competitiveness in addressing a range of image processing issues, such as foreground/background separation of color videos [12], color image denoising [13], edge detection [14], face recognition [15], and completion [4]. Specifically, the three color channels of a color image precisely correspond to the three imaginary sections of a quaternion matrix. We can express a pixel of a color image as a pure quaternion in the following manner:

$$\dot{p} = 0 + p_R i + p_G j + p_B k,$$

where p_R , p_G , and p_B correspond to the pixel values of the three channels (RGB) of a color pixel, respectively, and i , j , and k stand for the three imaginary units of a quaternion. Utilizing the pure quaternion matrix to represent the three color channels of a color image can better exploit the relationship between the channels in image processing. More recently, there have been proposed approaches that utilize quaternion-based LRMC for color image completion. A general approach is proposed in [16] for low-rank quaternion matrix completion (LRQMC) that employs the

quaternion nuclear norm (QNN) and three nonconvex rank surrogates. These surrogates rely on the Laplace function, Geman function, and weighted Schatten norm. These methods have demonstrated superior performance compared to some popular LRMC-based methods. However, they still require solving the singular values of a large quaternion matrix, which can significantly increase the algorithm’s computational complexity. Additionally, a logarithmic norm-based quaternion completion algorithm is proposed [17]. [18] proposed three minimization models based on quaternion-based bilinear decomposition. These approaches only require dealing with smaller-sized two-factor quaternion matrices, which reduces the computational complexity of solving quaternion singular value decomposition (QSVD). However, this factorization could result in getting trapped in a local minimum.

Indeed, the singular values and vectors can be obtained using the Qatar Riyal (QR) decomposition, which has lower algorithmic complexity than SVD [19]. Similarly, a method based on the quaternion QR (QQR) decomposition to approximate the QSVD of quaternion matrices (CQSVD-QQR) is also proposed [20]. Additionally, the $L_{2,1}$ -norm has recently shown success in various applications such as feature selection [21] and low-rank representation [22, 23, 19]. The study in [24] shows that the $L_{2,1}$ -norm provides better robustness against outliers. In low-rank representation, the $L_{2,1}$ -norm can be used to remove outliers by solving a minimization problem, which does not require the use of SVD to obtain the optimal solution [19]. However, currently, there is no quaternion $L_{2,1}$ -norm-based quaternion matrix completion method available. This inspired us to establish a quaternion-based color image completion model by introducing the quaternion $L_{2,1}$ -norm based on the quaternion Tri-Factorization method (CQSVD-QQR) so that the calculation of QSVD is not required during the model solving process.

In order to improve image completion results, it is essential to consider more information beyond just the low-rank qualities of images [25, 19]. One crucial factor is the sparsity of images in a particular domain, such as transform domains, where many signals have a naturally sparse structure. To address this, researchers have proposed combining low-rank and sparse priors. In [26], to formulate the sparse prior, the authors use the l_1 -norm regularizer, while the truncated nuclear norm is selected as the surrogate for the rank function. To extend this method to the quaternion system, the authors in [27] adapted it to work with quaternion matrices. Although combining low-rank and sparse prior has proven effective for improving image completion, these methods still depend on the SVD/QSVD calculation of large matrices, making them computationally expensive. We were inspired to improve the quaternion Tri-Factorization method (CQSVD-QQR)-based quaternion $L_{2,1}$ -norm minimization model by introducing the sparse regularization, which led to enhancing the precision of image completion results. The following points summarize the key contributions of this paper:

- A novel approach called QLNМ-QQR, based on quaternion $L_{2,1}$ -norm and CQSVD-QQR, is introduced for completing quaternion data. The computational complexity of QLNМ-QQR is reduced compared to methods

that use QSVD by replacing QSVD with QQR and the quaternion nuclear norm with the quaternion $L_{2,1}$ -norm.

- An improved method for quaternion matrix completion called IRQLNM-QQR is proposed by introducing iteratively reweighted quaternion $L_{2,1}$ -norm minimization. The proposed method enhances the accuracy of QLNM-QQR. Theoretical analysis demonstrates that IRQLNM-QQR achieves the same optimal solution as an LRQA-based method using the weighted Schatten function as the nonconvex rank surrogate, which outperforms the traditional QQR decomposition-based methods in terms of accuracy.
- To enhance the precision of color image recovery, we have integrated sparsity into the QLNM-QQR method, resulting in an improved method called QLNM-QQR-SR.
- We have proved that the quaternion $L_{2,1}$ -norm of a quaternion matrix serves as an upper bound for its quaternion nuclear norm. As a result, the methods proposed in this study can be extended to enhance the performance of low-rank representation and quaternion matrix completion methods based on the quaternion nuclear norm.

The structure of this paper is outlined as follows: Section 2 reviews the related models for completing matrices/quaternion matrices based on the low-rank property of data. Section 3 presents commonly used mathematical notations and provides a brief introduction to quaternion algebra. Section 4 gives a brief overview of the CQSVD-QQR technique, followed by the introduction of three proposed quaternion matrix-based completion algorithms. The computational complexities of the proposed models are also discussed. In Section 5, we provide experimental results and compare our proposed methods with several state-of-the-art approaches. Finally, Section 6 presents our conclusions.

2. Related work

A natural image has recurring patterns that may be utilized to estimate the missing values, which is the foundation for almost all of the existing image completion techniques [28, 29]. Consider an incomplete matrix $\mathbf{M} \in \mathbb{R}^{M \times N}$, $M \geq N > 0$. Following are the formulation for the conventional LRMC-based technique:

$$\min_{\mathbf{X}} \text{rank}(\mathbf{X}), \text{ s.t.}, P_{\Omega}(\mathbf{X} - \mathbf{M}) = \mathbf{0}, \quad (1)$$

where $\text{rank}(\cdot)$ signifies the rank function, $\mathbf{X} \in \mathbb{R}^{M \times N}$ represents a restored matrix, and Ω represents the set of observed entries. The definition of $P_\Omega(\mathbf{X})$ is given by

$$(P_\Omega(\mathbf{X}))_{mn} = \begin{cases} \mathbf{X}_{mn}, & (m, n) \in \Omega, \\ 0, & \text{otherwise.} \end{cases}$$

An effective method for solving the combinatorial optimization problem (1) is to optimize a convex substitute for the rank function. However, it should be noted that problem (1)-centric optimization algorithms mainly deal directly with two-dimensional data sets, specifically grayscale images. The processing of color images generally requires the RGB channels to be separated before the model in problem (1) can operate on them, while the LRQMC-based models can directly work with the assembled RGB channels. Analogous to problem (1) mentioned above, the prevalent low-rank quaternion matrix-based completion algorithm (LRQMC) can be expressed as follows:

$$\min_{\hat{\mathbf{X}}} \text{rank}(\hat{\mathbf{X}}), \text{ s.t.}, P_\Omega(\hat{\mathbf{X}} - \hat{\mathbf{M}}) = \mathbf{0}, \quad (2)$$

where $\hat{\mathbf{X}} \in \mathbb{H}^{M \times N}$ denotes the resulting quaternion matrix that has been completed, $\hat{\mathbf{M}} \in \mathbb{H}^{M \times N}$ is used to signify the observed quaternion matrix. The definition of $P_\Omega(\hat{\mathbf{X}})$ is given by

$$(P_\Omega(\hat{\mathbf{X}}))_{mn} = \begin{cases} \hat{\mathbf{X}}_{mn}, & (m, n) \in \Omega, \\ 0, & \text{otherwise.} \end{cases}$$

A commonly used technique for resolving the above minimization problem (2) is to adopt the QNN as a convex surrogate for the rank function. Subsequently, a minimization method can be formulated for this surrogate function as

$$\min_{\hat{\mathbf{X}}} \|\hat{\mathbf{X}}\|_*, \text{ s.t.}, P_\Omega(\hat{\mathbf{X}} - \hat{\mathbf{M}}) = \mathbf{0}, \quad (3)$$

where $\|\hat{\mathbf{X}}\|_*$ is the QNN of $\hat{\mathbf{X}}$.

Inspired by the favorable outcomes of nonconvex surrogates in LRMC, Chen *et al.* [16] present a universal LRQMC model as follows:

$$\min_{\hat{\mathbf{X}}} \sum_l \phi(\sigma_l(\hat{\mathbf{X}}), \gamma), \text{ s.t.}, P_\Omega(\hat{\mathbf{X}} - \hat{\mathbf{M}}) = \mathbf{0}, \quad (4)$$

where the nonnegative γ is associated with the particular function $\phi(\cdot)$. Furthermore, their proposed approaches are based on three nonconvex rank surrogates that utilize the Laplace, Geman, and Weighted Schatten- γ functions,

respectively. And

$$\|\dot{\mathbf{X}}\|_{L,\gamma} = \sum_l (1 - e^{-\frac{\sigma_l(\dot{\mathbf{X}})}{\gamma}}); \quad (5)$$

$$\|\dot{\mathbf{X}}\|_{G,\gamma} = \sum_l (1 - e^{-\frac{(1+\gamma)\sigma_l(\dot{\mathbf{X}})}{\gamma+\sigma_l(\dot{\mathbf{X}})}}); \quad (6)$$

$$\|\dot{\mathbf{X}}\|_{W,\gamma} = \sum_l \omega_l \sigma_l^\gamma(\dot{\mathbf{X}}). \quad (7)$$

As for $\|\dot{\mathbf{X}}\|_{W,\gamma}$, the contribution of the l -th singular value of $\dot{\mathbf{X}}$ ($\sigma_l(\dot{\mathbf{X}})$) to the quaternion rank is balanced using a non-negative weight scalar ω_l . LRQA-N, LRQA-L, LRQA-G, and LRQA-W are the four low-rank quaternion approximation (LRQA) methods proposed in [16], employing the nuclear norm, Laplace function, Geman function, and weighted Schatten norm, respectively. To gain a deeper insight, please consult [16].

3. Notations and preliminaries

The primary mathematical notations used in this paper are initially introduced in this part, and then some basic concepts and theorems in the quaternion system are provided. For a more in-depth understanding of quaternion algebra, we recommend reading [30].

3.1. Notations

\mathbb{R} , \mathbb{C} , and \mathbb{H} present the real space, complex space, and quaternion space, respectively. Lowercase letters, boldface lowercase letters, and boldface capital letters signify scalar, vectors, and matrices, respectively. A quaternion scalar, vector, and matrix are denoted by \dot{a} , $\dot{\mathbf{a}}$, $\dot{\mathbf{A}}$. $(\cdot)^T$, $(\cdot)^*$, and $(\cdot)^H$, respectively, signify the transpose, conjugation, and conjugate transpose. $|\cdot|$, $\|\cdot\|_1$, $\|\cdot\|_F$, and $\|\cdot\|_*$ correspond to the absolute value or modulus, the l_1 -norm, the Frobenius norm, and the nuclear norm, respectively. The trace and rank operators are denoted by $\text{tr}\{\cdot\}$ and $\text{rank}(\cdot)$, respectively. $\mathbf{I}_m \in \mathbb{R}^{m \times m}$ is the identity matrix. $\Re(\cdot)$ signifies its real part for a quaternion scalar, vector, or matrix.

3.2. The fundamentals of quaternion algebra

Quaternion is invented by Hamilton in 1843 [31]. The definition of quaternions is

$$\mathbb{H} = \{q_0 + q_1i + q_2j + q_3k | q_0, q_1, q_2, q_3 \in \mathbb{R}\} \quad (8)$$

and \mathbb{H} is an algebra that fulfills the associative law but not the commutative law. i, j, k in (8) represent imaginary units and satisfy $i^2 = j^2 = k^2 = ijk = -1$, and thus $ij = -ji = k, jk = -kj = i, ki = -ik = j$. Regarding any quaternion

$$\dot{q} = q_0 + q_1i + q_2j + q_3k = \Re(\dot{q}) + \Im(\dot{q}),$$

$\Re(\dot{q}) = q_0 \in \mathbb{R}$ is its real part and $\Im(\dot{q}) = q_1i + q_2j + q_3k$ is its vector part. Additionally, \dot{q} is referred to be a pure quaternion if $\Re(\dot{q}) = 0$. Obviously, in general, $\dot{p}\dot{q} \neq \dot{q}\dot{p}$ since the commutative property of multiplication does not apply to the quaternion algebra. Given \dot{q} , its conjugate is defined as $\dot{q}^* = q_0 - q_1i - q_2j - q_3k$, and its norm is calculated by $|\dot{q}| = \sqrt{\dot{q}^*\dot{q}} = \sqrt{q_0^2 + q_1^2 + q_2^2 + q_3^2}$.

For any quaternion matrix $\dot{\mathbf{Q}} = (\dot{q}_{mn}) \in \mathbb{H}^{M \times N}$, it can be expressed as $\dot{\mathbf{Q}} = \mathbf{Q}_0 + \mathbf{Q}_1i + \mathbf{Q}_2j + \mathbf{Q}_3k$, where $\mathbf{Q}_s \in \mathbb{R}^{M \times N}$ ($s = 0, 1, 2, 3$). If $\Re(\dot{\mathbf{Q}}) = \mathbf{Q}_0 = \mathbf{0}$, a quaternion matrix is referred to as a pure quaternion matrix. The following is the definition of a quaternion matrix $\dot{\mathbf{Q}}$'s Frobenius norm:

$$\|\dot{\mathbf{Q}}\|_F = \sqrt{\sum_{m=1}^M \sum_{n=1}^N |\dot{q}_{mn}|^2} = \sqrt{\text{tr}(\dot{\mathbf{Q}}^H \dot{\mathbf{Q}})}.$$

$\|\dot{\mathbf{Q}}\|_*$ denotes the nuclear norm of $\dot{\mathbf{Q}}$, and $\|\dot{\mathbf{Q}}\|_* = \sum_s \sigma_s(\dot{\mathbf{Q}})$, where $\sigma_s(\dot{\mathbf{Q}})$ is the s -th nonzero singular value of $\dot{\mathbf{Q}}$. The l_1 -norm of $\dot{\mathbf{Q}}$ is defined as $\|\dot{\mathbf{Q}}\|_1 = \sum_{m=1}^M \sum_{n=1}^N |\dot{q}_{mn}|$.

Definition 1 (Cayley-Dickson form [32] and Equivalent complex matrix of a quaternion matrix [33]). For any quaternion matrix $\dot{\mathbf{Q}} = \mathbf{Q}_0 + \mathbf{Q}_1i + \mathbf{Q}_2j + \mathbf{Q}_3k \in \mathbb{H}^{M \times N}$, its Cayley-Dickson form is given by $\dot{\mathbf{Q}} = \mathbf{Q}_a + \mathbf{Q}_bj$, where $\mathbf{Q}_a = \mathbf{Q}_0 + \mathbf{Q}_1i, \mathbf{Q}_b = \mathbf{Q}_2 + \mathbf{Q}_3i \in \mathbb{C}^{M \times N}$. And the following definition applies to its equivalent complex matrix $\chi_{\dot{\mathbf{Q}}} \in \mathbb{C}^{2M \times 2N}$:

$$\chi_{\dot{\mathbf{Q}}} = \begin{bmatrix} \mathbf{Q}_a & \mathbf{Q}_b \\ -\mathbf{Q}_b^* & \mathbf{Q}_a^* \end{bmatrix}. \quad (9)$$

There are many similarities between the quaternion matrix and its equivalent complex matrix. To learn more, we advise reading [33].

Theorem 1 (Quaternion singular value decomposition (QSVD) [33]). For every quaternion matrix $\dot{\mathbf{A}} \in \mathbb{H}^{M \times N}$ of rank r , two unitary quaternion matrices $\dot{\mathbf{U}} \in \mathbb{H}^{M \times M}$ and $\dot{\mathbf{V}} \in \mathbb{H}^{N \times N}$ exist, such that

$$\dot{\mathbf{A}} = \dot{\mathbf{U}} \begin{bmatrix} \Sigma_r & \mathbf{0} \\ \mathbf{0} & \mathbf{0} \end{bmatrix} \dot{\mathbf{V}}^H = \dot{\mathbf{U}} \Lambda \dot{\mathbf{V}}^H, \quad (10)$$

where Σ_r is a real diagonal matrix with r positive singular values of $\dot{\mathbf{A}}$ on its diagonal.

Theorem 2 (The quaternion Qatar Riyal decomposition (QQR) [34]). Considering an arbitrary quaternion matrix $\mathbf{\dot{A}} \in \mathbb{H}^{M \times N}$ with a rank of r , one can find a unitary quaternion matrix $\mathbf{\dot{Q}} \in \mathbb{H}^{M \times M}$ and a weakly upper triangular quaternion matrix $\mathbf{\dot{R}} \in \mathbb{H}^{M \times N}$, such that

$$\mathbf{\dot{A}} = \mathbf{\dot{Q}}\mathbf{\dot{R}}. \quad (11)$$

In other words, there exists a permutation matrix $\mathbf{P} \in \mathbb{R}^{N \times N}$ such that the product $\mathbf{\dot{R}}\mathbf{P}$ forms an upper triangular quaternion matrix.

lemma 1 ([16]). For any $\mu > 0$, $\mathbf{\dot{Y}} \in \mathbb{H}^{M \times N}$ is a given quaternion matrix and the QSVD of $\mathbf{\dot{Y}}$ is given by $\mathbf{\dot{Y}} = \mathbf{\dot{U}}\mathbf{\Sigma}\mathbf{\dot{V}}^H$. For the following quaternion nuclear norm minimization problem (QNNM)

$$\min_{\mathbf{\dot{X}}} \mu \|\mathbf{\dot{X}}\|_* + \frac{1}{2} \|\mathbf{\dot{Y}} - \mathbf{\dot{X}}\|_F^2, \quad (12)$$

the closed-form solution $\mathbf{\dot{\tilde{X}}}$ is given by

$$\mathbf{\dot{\tilde{X}}} = \mathbf{\dot{U}}S_\mu(\mathbf{\Sigma})\mathbf{\dot{V}}^H, \quad (13)$$

where $S_\mu(\mathbf{\Sigma}) = \text{diag}(\max\{\sigma_s(\mathbf{\dot{Y}}) - \mu, 0\})$ is the soft thresholding operator.

lemma 2 ([16]). Given a positive value of μ , $\mathbf{\dot{Y}} \in \mathbb{H}^{M \times N}$ is a known quaternion matrix, and its QSVD is expressed as $\mathbf{\dot{Y}} = \mathbf{\dot{U}}\mathbf{\Sigma}\mathbf{\dot{V}}^H$. The optimal solution for $\mathbf{\dot{\tilde{X}}}$ in the following problem

$$\min_{\mathbf{\dot{X}}} \mu \sum_l \omega_l \sigma_l(\mathbf{\dot{X}}) + \frac{1}{2} \|\mathbf{\dot{Y}} - \mathbf{\dot{X}}\|_F^2 \quad (14)$$

is given by

$$\mathbf{\dot{\tilde{X}}} = \mathbf{\dot{U}}\mathbf{\Sigma}_{\mathbf{\dot{X}}}\mathbf{\dot{V}}^H, \quad (15)$$

where $\mathbf{\Sigma}_{\mathbf{\dot{X}}} = \text{diag}(\sigma^*)$ and σ^* is given by

$$\sigma^* = \arg \min_{\sigma \geq 0} \mu \sum_l \omega_l \sigma_l(\mathbf{\dot{X}}) + \frac{1}{2} \|\sigma - \sigma_{\mathbf{\dot{Y}}}\|_F^2. \quad (16)$$

Presented below is a succinct overview of the Quaternion Discrete Cosine Transform.

Definition 2 (Forward quaternion discrete cosine transform (FQDCT) [35]). Given a quaternion matrix $\mathbf{\dot{A}} \in \mathbb{H}^{M \times N}$, as quaternions are non-commutative, its quaternion discrete cosine transform (QDCT) exists in two distinct types,

namely, the left-handed and right-handed forms as follows:

$$FQDCT^L(s, t) = \psi(s)\psi(t) \sum_{m=0}^{M-1} \sum_{n=0}^{N-1} \dot{q} \dot{\mathbf{A}}(m, n) Q(s, t, m, n), \quad (17)$$

$$FQDCT^R(s, t) = \psi(s)\psi(t) \sum_{m=0}^{M-1} \sum_{n=0}^{N-1} \dot{\mathbf{A}}(m, n) Q(s, t, m, n) \dot{q}, \quad (18)$$

where the pure quaternion \dot{q} , which fulfills the condition $\dot{q}^2 = -1$, is called the quaternionization factor. The values of $\psi(s)$, $\psi(t)$, and $Q(s, t, m, n)$ in the QDCT are similar to those in the discrete cosine transform (DCT) in the real domain, which are given as follows:

$$\psi(s) = \begin{cases} \sqrt{\frac{1}{M}} & \text{for } s = 0 \\ \sqrt{\frac{2}{M}} & \text{for } s \neq 0 \end{cases}, \quad \psi(t) = \begin{cases} \sqrt{\frac{1}{N}} & \text{for } t = 0 \\ \sqrt{\frac{2}{N}} & \text{for } t \neq 0 \end{cases}, \quad (19)$$

$$Q(s, t, m, n) = \cos\left[\frac{\pi(2m+1)s}{2M}\right] \cos\left[\frac{\pi(2n+1)t}{2N}\right]. \quad (20)$$

The two types of inverse QDCT (IQDCT), following the two forms of the FQDCT, are given below:

$$IQDCT^L(m, n) = \sum_{s=0}^{M-1} \sum_{t=0}^{N-1} \psi(s)\psi(t) \dot{q} \dot{\mathbf{B}}(s, t) Q(s, t, m, n), \quad (21)$$

$$IQDCT^R(m, n) = \sum_{s=0}^{M-1} \sum_{t=0}^{N-1} \psi(s)\psi(t) \dot{\mathbf{B}}(s, t) Q(s, t, m, n) \dot{q}, \quad (22)$$

where $\dot{\mathbf{B}} \in \mathbb{H}^{M \times N}$.

Theorem 3 (The relationship between FQDCT and IQDCT [35]).

$$\begin{aligned} \dot{\mathbf{A}}(m, n) &= IQDCT^L[FQDCT^L(\dot{\mathbf{A}}(m, n))] \\ &= IQDCT^R[FQDCT^R(\dot{\mathbf{A}}(m, n))]. \end{aligned} \quad (23)$$

Since the construction of our proposed model necessitates the use of $FQDCT^L$, we outline the computational steps of $FQDCT^L$ in the following.

1. Express the quaternion matrix $\dot{\mathbf{A}}(m, n) \in \mathbb{H}^{M \times N}$ in its Cayley-Dickson form, that is, $\dot{\mathbf{A}}(m, n) = \mathbf{A}_a(m, n) + \mathbf{A}_b(m, n)j$, where $\mathbf{A}_a(m, n)$ and $\mathbf{A}_b(m, n) \in \mathbb{C}^{M \times N}$.
2. Compute the DCT of $\mathbf{A}_a(m, n)$ and $\mathbf{A}_b(m, n)$, denoting the resulting matrices as $DCT(\mathbf{A}_a(m, n))$, and $DCT(\mathbf{A}_b(m, n))$,

respectively.

3. Using $DCT(\mathbf{A}_a(m, n))$ and $DCT(\mathbf{A}_b(m, n))$, construct a quaternion matrix $\hat{\mathbf{A}}(m, n)$ as follows: $\hat{\mathbf{A}}(m, n) = DCT(\mathbf{A}_a(m, n)) + DCT(\mathbf{A}_b(m, n))j$.
4. Multiply $\hat{\mathbf{A}}(m, n)$ by the quaternionization factor \dot{q} to obtain the final result:

$$FQDCT^L[\hat{\mathbf{A}}(m, n)] = \dot{q} \hat{\mathbf{A}}(m, n).$$

4. Our method of quaternion completion

After providing a brief overview of the CQSVD-QQR technique, this section introduces three novel algorithms for quaternion matrix-based completion. Furthermore, the computational complexities of these models are discussed.

4.1. A method for quaternion matrix decomposition

In the event that $\dot{\mathbf{X}} \in \mathbb{H}^{M \times N}$ is a quaternion matrix, the following quaternion Tri-Factorization is used to compute $\dot{\mathbf{X}}$'s approximation QSVD based on QQR decomposition (CQSVD-QQR) [20]:

$$\dot{\mathbf{X}} = \dot{\mathbf{L}}\dot{\mathbf{D}}\dot{\mathbf{R}}, \quad (24)$$

where the quaternion matrices $\dot{\mathbf{L}} \in \mathbb{H}^{M \times r}$ and $\dot{\mathbf{R}} \in \mathbb{H}^{r \times N}$ satisfy $\dot{\mathbf{L}}^H \dot{\mathbf{L}} = \mathbf{I}_r$, $\dot{\mathbf{R}} \dot{\mathbf{R}}^H = \mathbf{I}_r$, the quaternion matrix $\dot{\mathbf{D}} \in \mathbb{H}^{r \times r}$ is lower triangular, and $|D_{ss}| = |\sigma_s(\dot{\mathbf{X}})|$. The CQSVD-QQR procedure is briefly described below. For more information, please see [20]. First, suppose that $\dot{\mathbf{L}}^1 = \text{eye}(M, r)$, $\dot{\mathbf{D}}^1 = \text{eye}(r, r)$, and $\dot{\mathbf{R}}^1 = \text{eye}(r, N)$.

Next, in the $\tau + 1$ -th iteration, $\dot{\mathbf{L}}^{\tau+1}$ is determined by

$$[\dot{\mathbf{Q}}, \dot{\mathbf{G}}] = \text{qqr}(\dot{\mathbf{X}}(\dot{\mathbf{R}}^\tau)^H), \quad (25)$$

$$\dot{\mathbf{L}}^{\tau+1} = \dot{\mathbf{Q}}(:, 1 : r), \quad (26)$$

where the operator $\text{qqr}(\cdot)$ calculates the quaternion QR decomposition of a given quaternion matrix, and $\dot{\mathbf{Q}}(:, 1 : r)$ means to extract the first r columns of $\dot{\mathbf{Q}}$. $\dot{\mathbf{R}}^{\tau+1}$ is provided by

$$[\dot{\mathbf{T}}, \dot{\mathbf{S}}] = \text{qqr}(\dot{\mathbf{X}}^H \dot{\mathbf{L}}^{\tau+1}), \quad (27)$$

$$\dot{\mathbf{R}}^{\tau+1} = (\dot{\mathbf{T}}(:, 1 : r))^H. \quad (28)$$

The last update to $\dot{\mathbf{D}}^{\tau+1}$ is made by

$$\dot{\mathbf{D}}^{\tau+1} = (\dot{\mathbf{S}}(1:r, 1:r))^H, \quad (29)$$

4.2. Proposed three quaternion $L_{2,1}$ -norm-based methods for color image completion

The formulation of the proposed model is presented in this section. The definition of quaternion $L_{2,1}$ -norm of $\dot{\mathbf{X}} \in \mathbb{H}^{M \times N}$ is given by:

$$\|\dot{\mathbf{X}}\|_{2,1} = \sum_{n=1}^N \sqrt{\sum_{m=1}^M |\dot{\mathbf{X}}_{nm}|^2}. \quad (30)$$

We have verified that the three norm requirements are met by this valid norm, even for the triangle inequality.

For the quaternion $L_{2,1}$ -norm, we can obtain the following theorem.

Theorem 4. Using the method CQSVD-QQR, a quaternion matrix $\dot{\mathbf{X}} \in \mathbb{H}^{M \times N}$ can be decomposed into $\dot{\mathbf{X}} = \dot{\mathbf{L}}\dot{\mathbf{D}}\dot{\mathbf{R}}$. And for $\|\dot{\mathbf{D}}\|_*$ and $\|\dot{\mathbf{D}}\|_{2,1}$, it can be found that $\|\dot{\mathbf{D}}\|_* \leq \|\dot{\mathbf{D}}\|_{2,1}$.

Proof. The following is a decomposition of the quaternion matrix $\dot{\mathbf{D}} \in \mathbb{H}^{r \times r}$:

$$\dot{\mathbf{D}} = \sum_{l=1}^r \dot{\mathbf{D}}^l, \quad (31)$$

$$\dot{\mathbf{D}}^l_{ts} = \begin{cases} \dot{\mathbf{D}}_{tl}, & (s = l), \\ 0, & (s \neq l), \end{cases} \quad (32)$$

where $\dot{\mathbf{D}}^l \in \mathbb{H}^{r \times r}$, and $t, s = 1, \dots, r$. Due to the convex nature of the quaternion nuclear norm, we can obtain that

$$\|\dot{\mathbf{D}}\|_* \leq \sum_{l=1}^r \|\dot{\mathbf{D}}^l\|_*, \quad (33)$$

By calculating the singular values of the equivalent complex matrix of $\dot{\mathbf{D}}^l$ and according to the definition of the QNN, we can get

$$\|\dot{\mathbf{D}}^l\|_* = \sqrt{\sum_{t=1}^r |\dot{\mathbf{D}}_{tl}|^2}. \quad (34)$$

According to (34), we have

$$\sum_{l=1}^r \|\dot{\mathbf{D}}^l\|_* = \|\dot{\mathbf{D}}\|_{2,1}. \quad (35)$$

Therefore, we proved the above conclusion. \square

1) *The proposed CQSVD-QQR-based quaternion $L_{2,1}$ -norm minimization approach:* The quaternion $L_{2,1}$ -norm of

a quaternion matrix is unquestionably the upper bound of its QNN, as shown by Theorem (4). This result inspires us to replace the QNN in the minimization problem of (3) with the quaternion $L_{2,1}$ -norm for quaternion matrix completion in the manner described below:

$$\min_{\mathbf{D}} \|\mathbf{D}\|_{2,1}, \text{ s.t., } \begin{cases} \mathbf{L}^H \mathbf{L} = \mathbf{I}_r, \mathbf{R} \mathbf{R}^H = \mathbf{I}_r, \\ \mathbf{X} = \mathbf{L} \mathbf{D} \mathbf{R}, P_{\Omega}(\mathbf{L} \mathbf{D} \mathbf{R} - \mathbf{M}) = \mathbf{0}. \end{cases} \quad (36)$$

Convexity of the quaternion $L_{2,1}$ -norm in the optimization function in (36) allows for the solution of the problem using the alternating direction method of multipliers (ADMM). And we give the augmented Lagrangian function of (36):

$$\text{Lag} = \|\mathbf{D}\|_{2,1} + \Re(\langle \mathbf{E}, \mathbf{X} - \mathbf{L} \mathbf{D} \mathbf{R} \rangle) + \frac{\mu}{2} \|\mathbf{X} - \mathbf{L} \mathbf{D} \mathbf{R}\|_F^2, \quad (37)$$

where $\mu > 0$, and the lagrange multiplier $\mathbf{E} \in \mathbb{H}^{M \times N}$. Essentially, there are two steps in the process of solving the entire problem. The first step is to update the variables \mathbf{L} and \mathbf{R} by solving the corresponding optimization problem based on the CQSVD-QQR method. The second step involves updating the variables \mathbf{D} and \mathbf{X} .

The following minimization problem is solved in step 1 to update $\mathbf{L}^{\tau+1}$ and $\mathbf{R}^{\tau+1}$:

$$\min_{\mathbf{L}, \mathbf{R}} \left\| (\mathbf{X}^{\tau} + \mathbf{E}^{\tau} / \mu^{\tau}) - \mathbf{L} \mathbf{D}^{\tau} \mathbf{R} \right\|_F^2. \quad (38)$$

We can update $\mathbf{L}^{\tau+1}$ and $\mathbf{R}^{\tau+1}$ by using CQSVD-QQR, in accordance with the analysis of the CQSVD-QQR method, i.e.,

$$\begin{cases} \left[\hat{\mathbf{L}}^{\tau+1}, \sim \right] = \text{qqr}(\hat{\mathbf{X}}_b (\mathbf{R}^{\tau})^H), \\ \mathbf{L}^{\tau+1} = \hat{\mathbf{L}}^{\tau+1}(:, 1 : r), \end{cases} \quad (39)$$

and

$$\begin{cases} \left[\hat{\mathbf{R}}^{\tau+1}, \hat{\mathbf{D}}^{\tau} \right] = \text{qqr}(\hat{\mathbf{X}}_b^H \mathbf{L}^{\tau+1}), \\ \mathbf{R}^{\tau+1} = (\hat{\mathbf{R}}^{\tau+1}(1 : r, 1 : r))^H, \end{cases} \quad (40)$$

where $\hat{\mathbf{X}}_b = \mathbf{X}^{\tau} + \mathbf{E}^{\tau} / \mu^{\tau}$. If \mathbf{L} and \mathbf{R} are initialized as \mathbf{L}^{τ} and \mathbf{R}^{τ} , the CQSVD-QQR method will converge within a limited number of iterations since the quaternion matrices \mathbf{L} and \mathbf{R} do not change significantly during the course of two iterations [19]. Therefore, the experiment's good outcome and the speed at which our algorithm iterates may both be enhanced by employing this wise initialization.

Step 2 involves updating $\mathbf{D}^{\tau+1}$ and $\mathbf{X}^{\tau+1}$. The following quaternion $L_{2,1}$ -norm minimization problem is needed to

solve in order to determine $\dot{\mathbf{D}}^{\tau+1}$:

$$\dot{\mathbf{D}}^{\tau+1} = \arg \min_{\mathbf{D}} \|\dot{\mathbf{D}}\|_{2,1} + \frac{\mu^\tau}{2} \|\dot{\mathbf{D}} - (\dot{\mathbf{L}}^{\tau+1})^H \dot{\mathbf{X}}_b (\dot{\mathbf{R}}^{\tau+1})^H\|_F^2. \quad (41)$$

The following theorem is established in order to solve the above problem (41).

Theorem 5. For the following minimization problem

$$\min_{\dot{\mathbf{X}}} \mathcal{J}(\dot{\mathbf{X}}) = \min_{\dot{\mathbf{X}}} \beta \|\dot{\mathbf{X}}\|_{2,1} + \frac{1}{2} \|\dot{\mathbf{X}} - \dot{\mathbf{Y}}\|_F^2, \quad (42)$$

where $\beta > 0$, $\dot{\mathbf{X}}$, and $\dot{\mathbf{Y}} \in \mathbb{H}^{M \times N}$, the n -th column of the optimal $\tilde{\dot{\mathbf{X}}}$, i.e., $\tilde{\dot{\mathbf{X}}}_n$, of (42) is given by

$$\tilde{\dot{\mathbf{X}}}_n = \frac{(\|\dot{\mathbf{Y}}_{\cdot n}\|_2 - 4\beta)_+ \dot{\mathbf{Y}}_{\cdot n}}{\|\dot{\mathbf{Y}}_{\cdot n}\|_2}, \quad (43)$$

where $\tilde{\dot{\mathbf{X}}}_n = [\tilde{\dot{\mathbf{X}}}_{1n}, \tilde{\dot{\mathbf{X}}}_{2n}, \dots, \tilde{\dot{\mathbf{X}}}_{Mn}]^T$, $\|\dot{\mathbf{Y}}_{\cdot n}\|_2 = \sqrt{\sum_{m=1}^M |\dot{\mathbf{Y}}_{mn}|^2}$, and $(\|\dot{\mathbf{Y}}_{\cdot n}\|_2 - 4\beta)_+ = \max\{\|\dot{\mathbf{Y}}_{\cdot n}\|_2 - 4\beta, 0\}$.

The proof of Theorem 5 can be found in the [Appendix A](#).

Therefore, we can update $\dot{\mathbf{D}}^{\tau+1}$ in the problem (41) by using Theorem 5 as follows:

$$\dot{\mathbf{D}}^{\tau+1} = \hat{\mathbf{D}} \mathbf{C}, \quad (44)$$

where $\hat{\mathbf{D}} = (\dot{\mathbf{L}}^{\tau+1})^H \dot{\mathbf{X}}_b (\dot{\mathbf{R}}^{\tau+1})^H$, and $\mathbf{C} = \text{diag}(c_1, \dots, c_r)$ is a diagonal matrix, where c_s ($s = 1, \dots, r$) is given by

$$c_s = \frac{(\|\hat{\mathbf{D}}_{\cdot s}\|_2 - 4\beta)_+}{\|\hat{\mathbf{D}}_{\cdot s}\|_2}. \quad (45)$$

Next, we can update the variable $\dot{\mathbf{X}}_{\tau+1}$ by fixing the other variables as follows:

$$\dot{\mathbf{X}}^{\tau+1} = \dot{\mathbf{L}}^{\tau+1} \dot{\mathbf{D}}^{\tau+1} \dot{\mathbf{R}}^{\tau+1} - P_{\Omega}(\dot{\mathbf{L}}^{\tau+1} \dot{\mathbf{D}}^{\tau+1} \dot{\mathbf{R}}^{\tau+1}) + P_{\Omega}(\dot{\mathbf{M}}). \quad (46)$$

Finally, we can update $\dot{\mathbf{E}}^{\tau+1}$ and μ by fixing the variables $\dot{\mathbf{L}}^{\tau+1}$, $\dot{\mathbf{D}}^{\tau+1}$, $\dot{\mathbf{R}}^{\tau+1}$, and $\dot{\mathbf{X}}^{\tau+1}$ as follows:

$$\dot{\mathbf{E}}^{\tau+1} = \dot{\mathbf{E}}^{\tau} + \mu^\tau (\dot{\mathbf{X}}^{\tau+1} - \dot{\mathbf{L}}^{\tau+1} \dot{\mathbf{D}}^{\tau+1} \dot{\mathbf{R}}^{\tau+1}), \quad (47)$$

$$\mu^{\tau+1} = \rho \mu^\tau, \quad (48)$$

where $\rho \geq 1$. We call the proposed CQSVD-QQR-based quaternion $L_{2,1}$ -norm minimization approach QLNМ-QQR. Algorithm 1 provides a summary of the whole proposed approach's process.

QLNM-QQR can reach its optimal solution because the ADMM, a gradient-search-based approach, minimizes

Algorithm 1 The QLNМ-QQR method for color image completion.

Input: The observed quaternion matrix data $\mathbf{M} \in \mathbb{H}^{M \times N}$ with $\mathcal{P}_{\Omega^c}(\mathbf{M}) = \mathbf{0}$; μ_{\max} ; ρ and $r > 0$.

1: **Initialize** $\tau = 0$; μ^0 ; $\varepsilon > 0$; $\text{It}_{\max} > 0$; $\mathbf{L}^0 = \text{eye}(M, r)$; $\mathbf{R}^0 = \text{eye}(r, N)$; $\mathbf{D}^0 = \text{eye}(r, r)$; $\mathbf{X}^0 = \mathbf{M}$.

2: **Repeat**

3: **Step 1.** $\mathbf{L}^{\tau+1}$, $\mathbf{R}^{\tau+1}$: (39) and (40), respectively.

4: **Step 2.** $\mathbf{D}^{\tau+1}$: (44) and (45).

5: **Step 3.** $\mathbf{X}^{\tau+1} = \mathbf{L}^{\tau+1} \mathbf{D}^{\tau+1} \mathbf{R}^{\tau+1} - P_{\Omega}(\mathbf{L}^{\tau+1} \mathbf{D}^{\tau+1} \mathbf{R}^{\tau+1}) + P_{\Omega}(\mathbf{M})$.

6: $\mathbf{E}^{\tau+1} = \mathbf{E}^{\tau} + \mu^{\tau}(\mathbf{X}^{\tau+1} - \mathbf{L}^{\tau+1} \mathbf{D}^{\tau+1} \mathbf{R}^{\tau+1})$.

7: $\mu^{\tau+1} = \min(\rho \mu^{\tau}, \mu_{\max})$.

8: **Until convergence**

Output: $\mathbf{L}^{\tau+1}$, $\mathbf{D}^{\tau+1}$, $\mathbf{R}^{\tau+1}$, and $\mathbf{X}^{\tau+1}$.

the convex optimization function of (36) and thus allows for convergence. Assume that QLNМ-QQR converges after t iterations. If the updating processes of the QLNМ-QQR approach are carried out further, \mathbf{X}^{τ} ($\tau \geq t$) will equal \mathbf{X}^t . QLNМ-QQR can revert to CQSVD-QQR since \mathbf{L} and \mathbf{R} from the preceding iteration served as initialization for CQSVD-QQR. Consequently, the series of $\{\mathbf{D}^{\tau}\}$ generated by QLNМ-QQR will converge to a diagonal matrix \mathbf{D} and

$$|\mathbf{D}_{ss}| = \sigma_s(\mathbf{X}^t). \quad (49)$$

Because of this, the QLNМ-QQR algorithm's quaternion $L_{2,1}$ -norm minimization function can reach the QNN of \mathbf{D} . It inspires us to extend QLNМ-QQR by introducing a quaternion $L_{2,1}$ -norm minimization approach with iterative reweighting.

2) *Extending the approach QLNМ-QQR with iterative reweighting:* Based on (35), the weighted quaternion $L_{2,1}$ -norm of $\mathbf{X} \in \mathbb{H}^{M \times N}$ is given by

$$\|\mathbf{X}\|_{\omega, (2,1)} = \sum_{l=1}^N \omega_l \|\mathbf{X}^l\|_*, \quad (50)$$

where ω_l is a positive number, and \mathbf{X}^l and \mathbf{D}^l (in (31)) both have the same definition. The following modification can be made to the QLNМ-QQR minimization problem in (36):

$$\min_{\mathbf{D}} \sum_{l=1}^r \partial g(\|\mathbf{D}^l\|_*) \|\mathbf{D}^l\|_*, \text{ s.t., } \begin{cases} \mathbf{L}^H \mathbf{L} = \mathbf{I}_r, \quad \mathbf{R} \mathbf{R}^H = \mathbf{I}_r, \\ \mathbf{X} = \mathbf{L} \mathbf{D} \mathbf{R}, \quad P_{\Omega}(\mathbf{L} \mathbf{D} \mathbf{R} - \mathbf{M}) = \mathbf{0}. \end{cases} \quad (51)$$

$\partial g(\sigma_s)$ is the gradient of $g(\cdot)$ at σ_s , and $g(\cdot)$ is continuous, concave, smooth, differentiable, and monotonically increas-

ing on $[0, +\infty)$ [19, 16]. The ADMM can resolve the problem in (51). We give its augmented Lagrangian function as below:

$$\begin{aligned} & \mathcal{L}(\dot{\mathbf{X}}, \dot{\mathbf{L}}, \dot{\mathbf{D}}, \dot{\mathbf{R}}, \dot{\mathbf{Y}}) \\ &= \sum_{l=1}^r \partial g(\|\dot{\mathbf{D}}^l\|_*) \|\dot{\mathbf{D}}^l\|_* + \Re(\langle \dot{\mathbf{E}}, \dot{\mathbf{X}} - \dot{\mathbf{L}}\dot{\mathbf{D}}\dot{\mathbf{R}} \rangle) + \frac{\mu}{2} \|\dot{\mathbf{X}} - \dot{\mathbf{L}}\dot{\mathbf{D}}\dot{\mathbf{R}}\|_F^2, \end{aligned} \quad (52)$$

In the τ -th iteration, the variables $\dot{\mathbf{X}}^{\tau+1}$, $\dot{\mathbf{L}}^{\tau+1}$, $\dot{\mathbf{R}}^{\tau+1}$, $\dot{\mathbf{E}}^{\tau+1}$, and $\mu^{\tau+1}$ are updated the same as we did in the previous problem (36). We need to solve the subsequent minimization problem to update $\dot{\mathbf{D}}^{\tau+1}$:

$$\min_{\dot{\mathbf{D}}} \sum_{l=1}^r \partial g(\|\dot{\mathbf{D}}^l\|_*) \|\dot{\mathbf{D}}^l\|_* + \frac{\mu^\tau}{2} \|\dot{\mathbf{D}} - \dot{\mathbf{D}}\|_F^2, \quad (53)$$

where $\dot{\mathbf{D}} = (\dot{\mathbf{L}}^{\tau+1})^H \dot{\mathbf{X}}_b (\dot{\mathbf{R}}^{\tau+1})^H$. As in [19], in the τ -th iteration, we also let

$$\partial g(\|\dot{\mathbf{D}}^l\|_*) = \mu^\tau (1 - \hat{a}_l) \|\dot{\mathbf{D}}^l\|_* \quad (l = 1, 2, \dots, r) \quad (54)$$

where $1 \geq \hat{a}_1 \geq \hat{a}_2 \geq \dots \geq \hat{a}_r > 0$.

Theorem 6. Assume that $\dot{\mathbf{Y}} \in \mathbb{H}^{M \times M}$ and $\mu > 0$, for the minimization problem below,

$$\min_{\dot{\mathbf{X}} \in \mathbb{H}^{M \times M}} \frac{1}{\mu} \|\dot{\mathbf{X}}\|_{\omega(2,1)} + \frac{1}{2} \|\dot{\mathbf{X}} - \dot{\mathbf{Y}}\|_F^2, \quad (55)$$

the optimal solution is given by

$$\dot{\mathbf{X}}_{\text{opt}} = \dot{\mathbf{Y}}\mathbf{A}, \quad (56)$$

where $\mathbf{A} = \text{diag}(a_1, \dots, a_M)$, and

$$a_m = \frac{(\sigma_m - \frac{\omega_m}{\mu})_+}{\sigma_m}, \quad (m = 1, \dots, M) \quad (57)$$

where σ_m is the singular value of $\dot{\mathbf{Y}}^m$. $\dot{\mathbf{Y}}^m$ is defined in the same way as $\dot{\mathbf{D}}^l$ in (31).

The proof of Theorem 6 can be found in the [Appendix B](#).

Theorem 6 and (54) allow us to update $\dot{\mathbf{D}}^{\tau+1}$ as follows:

$$\dot{\mathbf{D}}^{\tau+1} = \dot{\mathbf{D}}\mathbf{A}, \quad (58)$$

where $\mathbf{A} = \text{diag}(\hat{a}_1, \dots, \hat{a}_r)$. We abbreviate the proposed CQSVD-QQR-based iteratively reweighted quaternion $L_{2,1}$ -

norm minimization model for matrix completion as IRQLNM-QQR.

Theorem 7. By using (54) to specify the weights $\partial g(\|\mathbf{D}^l\|_*)$ ($l = 1, \dots, r$) in (52), IRQLNM-QQR can converge to the optimal solution of an LRQA-W minimization model with $\gamma = 1$.

The proof of Theorem 7 can be found in the Appendix C.

For the experiment, we have specified the values of \hat{a}_l ($l = 1, 2, \dots, r$) as follows:

$$\omega_l = \begin{cases} 1, & 1 \leq l \leq V, 1 < V < r \\ \frac{\varsigma-1}{r-V} + \omega_{l-1}, & V < l \leq r, \end{cases} \quad (59)$$

$$\hat{a}_l = \frac{1}{\omega_l} \quad (60)$$

where $\varsigma > 1$, r represents the number of rows in \mathbf{A} from (58).

3) *QLNM-QQR with sparsity*: As we previously indicated, the performance of color image completion models will be enhanced by combining the low-rank property of color images with sparsity. As a result, we introduce the sparse regularization term into the minimization problem (36) and have the following optimization problem:

$$\min_{\mathbf{D}} \|\mathbf{D}\|_{2,1} + \beta \|\mathbf{C}\|_1, \text{ s.t., } \begin{cases} \mathbf{L}^H \mathbf{L} = \mathbf{I}_r, \mathbf{R} \mathbf{R}^H = \mathbf{I}_r, \\ \mathbf{X} = \mathbf{L} \mathbf{D} \mathbf{R}, P_{\Omega}(\mathbf{L} \mathbf{D} \mathbf{R}) = P_{\Omega}(\mathbf{M}), \mathcal{T}(\mathbf{X}) = \mathbf{C}, \end{cases} \quad (61)$$

where $\beta > 0$, $\mathbf{C} = \mathcal{T}(\mathbf{X})$ stands for the quaternion matrix after transformation, and $\mathcal{T}(\cdot)$ denotes a transform operator. In this section, the FQDCT^L is employed to formulate our proposed approach. In this case, $\mathcal{T}(\mathbf{X})$ calculates FQDCT^L of \mathbf{X} .

We also use the ADMM framework in the quaternion system to solve problem (61), and its corresponding augmented Lagrangian function is shown below:

$$\text{Lag} = \|\mathbf{D}\|_{2,1} + \beta \|\mathbf{C}\|_1 + \Re(\langle \mathbf{E}, \mathbf{X} - \mathbf{L} \mathbf{D} \mathbf{R} \rangle) + \frac{\mu}{2} \|\mathbf{X} - \mathbf{L} \mathbf{D} \mathbf{R}\|_F^2 + \Re(\langle \mathbf{F}, \mathbf{C} - \mathcal{T}(\mathbf{X}) \rangle) + \frac{\mu}{2} \|\mathbf{C} - \mathcal{T}(\mathbf{X})\|_F^2, \quad (62)$$

where the penalty parameter μ is a positive number, \mathbf{E} and \mathbf{F} are Lagrange multiplier. The ADMM framework allows for the alternate updating of each parameter in the optimization problem (61) by fixing other variables. Notably, in

the τ -th iteration, each variable can be updated as follows:

$$\left\{ \begin{array}{l} \dot{\mathbf{L}}^{\tau+1} = \arg \min_{\mathbf{L}} \text{Lag}(\dot{\mathbf{X}}^{\tau}, \dot{\mathbf{L}}, \dot{\mathbf{D}}^{\tau}, \dot{\mathbf{R}}^{\tau}, \dot{\mathbf{C}}^{\tau}, \dot{\mathbf{E}}^{\tau}, \dot{\mathbf{F}}^{\tau}), \\ \dot{\mathbf{R}}^{\tau+1} = \arg \min_{\mathbf{R}} \text{Lag}(\dot{\mathbf{X}}^{\tau}, \dot{\mathbf{L}}^{\tau+1}, \dot{\mathbf{D}}^{\tau}, \dot{\mathbf{R}}, \dot{\mathbf{C}}^{\tau}, \dot{\mathbf{E}}^{\tau}, \dot{\mathbf{F}}^{\tau}), \\ \dot{\mathbf{D}}^{\tau+1} = \arg \min_{\mathbf{D}} \text{Lag}(\dot{\mathbf{X}}^{\tau}, \dot{\mathbf{L}}^{\tau+1}, \dot{\mathbf{D}}, \dot{\mathbf{R}}^{\tau+1}, \dot{\mathbf{C}}^{\tau}, \dot{\mathbf{E}}^{\tau}, \dot{\mathbf{F}}^{\tau}), \\ \dot{\mathbf{X}}^{\tau+1} = \arg \min_{\mathbf{X}} \text{Lag}(\dot{\mathbf{X}}, \dot{\mathbf{L}}^{\tau+1}, \dot{\mathbf{D}}^{\tau+1}, \dot{\mathbf{R}}^{\tau+1}, \dot{\mathbf{C}}^{\tau}, \dot{\mathbf{E}}^{\tau}, \dot{\mathbf{F}}^{\tau}), \\ \dot{\mathbf{C}}^{\tau+1} = \arg \min_{\mathbf{C}} \text{Lag}(\dot{\mathbf{X}}^{\tau+1}, \dot{\mathbf{L}}^{\tau+1}, \dot{\mathbf{D}}^{\tau+1}, \dot{\mathbf{R}}^{\tau+1}, \dot{\mathbf{C}}, \dot{\mathbf{E}}^{\tau}, \dot{\mathbf{F}}^{\tau}), \\ \dot{\mathbf{E}}^{\tau+1} = \dot{\mathbf{E}}^{\tau} + \mu^{\tau}(\dot{\mathbf{X}}^{\tau+1} - \dot{\mathbf{L}}^{\tau+1}\dot{\mathbf{D}}^{\tau+1}\dot{\mathbf{R}}^{\tau+1}), \\ \dot{\mathbf{F}}^{\tau+1} = \dot{\mathbf{F}}^{\tau} + \mu^{\tau}(\dot{\mathbf{C}}^{\tau+1} - \mathcal{T}(\dot{\mathbf{X}}^{\tau+1})). \end{array} \right. \quad (63)$$

Updating $\dot{\mathbf{L}}$, $\dot{\mathbf{D}}$, and $\dot{\mathbf{R}}$: The following minimization problem is needed to solve in the $\tau + 1$ -th iteration to update $\dot{\mathbf{L}}^{\tau+1}$ and $\dot{\mathbf{R}}^{\tau+1}$:

$$\min_{\mathbf{L}, \mathbf{R}} \left\| \left(\dot{\mathbf{X}}^{\tau} + \frac{\dot{\mathbf{E}}^{\tau}}{\mu^{\tau}} \right) - \dot{\mathbf{L}}\dot{\mathbf{D}}^{\tau}\dot{\mathbf{R}} \right\|_F^2. \quad (64)$$

The updates of $\dot{\mathbf{L}}^{\tau+1}$ and $\dot{\mathbf{R}}^{\tau+1}$ here are the same as in the QLM-QQR method, i.e., $\dot{\mathbf{L}}^{\tau+1}$ and $\dot{\mathbf{R}}^{\tau+1}$ are updated according to (39) and (40), respectively.

Also, since variable $\dot{\mathbf{D}}$ does not directly rely on variable $\dot{\mathbf{C}}$, $\dot{\mathbf{D}}^{\tau+1}$ is updated by addressing the same problem, i.e., problem (41), in the previous subsection. Thus, we update $\dot{\mathbf{D}}^{\tau+1}$ by using (44).

Updating $\dot{\mathbf{X}}$, $\dot{\mathbf{C}}$, $\dot{\mathbf{E}}$, $\dot{\mathbf{F}}$, and μ : By resolving the following problem in the τ -th iteration, $\dot{\mathbf{X}}^{\tau+1}$ can be updated after updating the variables $\dot{\mathbf{L}}^{\tau+1}$, $\dot{\mathbf{D}}^{\tau+1}$, and $\dot{\mathbf{R}}^{\tau+1}$ and fixing the remaining variables:

$$\begin{aligned} \dot{\mathbf{X}}^{\tau+1} &= \arg \min_{\mathbf{X}} \Re(\langle \dot{\mathbf{E}}^{\tau}, \dot{\mathbf{X}} - \dot{\mathbf{L}}^{\tau+1}\dot{\mathbf{D}}^{\tau+1}\dot{\mathbf{R}}^{\tau+1} \rangle) + \frac{\mu^{\tau}}{2} \|\dot{\mathbf{X}} - \dot{\mathbf{L}}^{\tau+1}\dot{\mathbf{D}}^{\tau+1}\dot{\mathbf{R}}^{\tau+1}\|_F^2 \\ &\quad + \Re(\langle \dot{\mathbf{F}}^{\tau}, \dot{\mathbf{C}}^{\tau} - \mathcal{T}(\dot{\mathbf{X}}) \rangle) + \frac{\mu^{\tau}}{2} \|\dot{\mathbf{C}}^{\tau} - \mathcal{T}(\dot{\mathbf{X}})\|_F^2, \\ &= \arg \min_{\mathbf{X}} \frac{\mu^{\tau}}{2} \|\dot{\mathbf{X}} + \frac{\dot{\mathbf{E}}^{\tau}}{\mu^{\tau}} - \dot{\mathbf{L}}^{\tau+1}\dot{\mathbf{D}}^{\tau+1}\dot{\mathbf{R}}^{\tau+1}\|_F^2 + \frac{\mu^{\tau}}{2} \|\dot{\mathbf{C}}^{\tau} + \frac{\dot{\mathbf{F}}^{\tau}}{\mu^{\tau}} - \mathcal{T}(\dot{\mathbf{X}})\|_F^2. \end{aligned} \quad (65)$$

Since the item $\mathcal{T}(\dot{\mathbf{X}})$ is contained in problem (65), we cannot direct separate variable $\dot{\mathbf{X}}$ from other variables. We can reformulate the problem according to the Parseval theorem in the quaternion system, and then we can isolate $\dot{\mathbf{X}}$ from $\mathcal{T}(\cdot)$. The quaternion system's equivalent of the Parseval theorem in the real domain states that following a unitary transformation like the quaternion discrete Fourier transform (QDFT) or quaternion discrete cosine transform (QDCT), the signal's overall energy stays constant [36]. As a result, by adding the appropriate inverse transform to

the final component in (65), we get that

$$\|\dot{\mathbf{C}}^\tau + \frac{\dot{\mathbf{F}}^\tau}{\mu^\tau} - \mathcal{T}(\dot{\mathbf{X}})\|_F^2 = \|\mathcal{I}(\dot{\mathbf{C}}^\tau + \frac{\dot{\mathbf{F}}^\tau}{\mu^\tau}) - \dot{\mathbf{X}}\|_F^2, \quad (66)$$

where $\mathcal{I}(\cdot)$ stands for $\mathcal{T}(\cdot)$'s inverse transform. According to (65) and (66), as seen below, the optimization problem that is used to update \mathbf{X} is reformulated as:

$$\dot{\mathbf{X}}^{\tau+1} = \arg \min_{\dot{\mathbf{X}}} \left\| \frac{1}{2}(\dot{\mathbf{L}}^{\tau+1}\dot{\mathbf{D}}^{\tau+1}\dot{\mathbf{R}}^{\tau+1} + \mathcal{I}(\dot{\mathbf{C}}^\tau + \frac{\dot{\mathbf{F}}^\tau}{\mu^\tau}) - \frac{\dot{\mathbf{E}}^\tau}{\mu^\tau}) - \dot{\mathbf{X}} \right\|_F^2. \quad (67)$$

The closed-form solution to the problem (67) is given by

$$\dot{\mathbf{X}}^{\tau+1} = \frac{1}{2}(\dot{\mathbf{L}}^{\tau+1}\dot{\mathbf{D}}^{\tau+1}\dot{\mathbf{R}}^{\tau+1} + \mathcal{I}(\dot{\mathbf{C}}^\tau + \frac{\dot{\mathbf{F}}^\tau}{\mu^\tau}) - \frac{\dot{\mathbf{E}}^\tau}{\mu^\tau}). \quad (68)$$

Considering the restriction $P_\Omega(\dot{\mathbf{L}}\dot{\mathbf{D}}\dot{\mathbf{R}}) = P_\Omega(\dot{\mathbf{M}})$, we get that

$$\dot{\mathbf{X}}^{\tau+1} = P_\Omega(\dot{\mathbf{M}}) + P_{\Omega^c}(\dot{\mathbf{X}}^{\tau+1}), \quad (69)$$

where Ω^c stands for the missing entries' indexes.

The next step is to update the variable $\dot{\mathbf{C}}^{\tau+1}$ by resolving the following problem:

$$\begin{aligned} \dot{\mathbf{C}}^{\tau+1} &= \arg \min_{\dot{\mathbf{C}}} \beta \|\dot{\mathbf{C}}\|_1 + \Re(\langle \dot{\mathbf{F}}^\tau, \dot{\mathbf{C}} - \mathcal{T}(\dot{\mathbf{X}}^{\tau+1}) \rangle) + \frac{\mu^\tau}{2} \|\dot{\mathbf{C}} - \mathcal{T}(\dot{\mathbf{X}}^{\tau+1})\|_F^2 \\ &= \arg \min_{\dot{\mathbf{C}}} \beta \|\dot{\mathbf{C}}\|_1 + \frac{\mu^\tau}{2} \left\| \frac{\dot{\mathbf{F}}^\tau}{\mu^\tau} + \dot{\mathbf{C}} - \mathcal{T}(\dot{\mathbf{X}}^{\tau+1}) \right\|_F^2. \end{aligned} \quad (70)$$

The closed-form solution to the problem (70) is given by

$$\dot{\mathbf{C}}^{\tau+1} = \mathcal{S}_{\frac{\beta}{\mu^\tau}}(\mathcal{T}(\dot{\mathbf{X}}^{\tau+1}) - \frac{\dot{\mathbf{F}}^\tau}{\mu^\tau}), \quad (71)$$

where $\mathcal{S}_t(\mathbf{x}) = \frac{\mathbf{x}}{|\mathbf{x}|} \max\{|\mathbf{x}| - t, 0\}$ stands for the element-wise soft thresholding operator [27].

Finally, the penalty parameter $\mu^{\tau+1}$ is updated as follows:

$$\mu^{\tau+1} = \rho \mu^\tau. \quad (72)$$

We call this approach QLNМ-QQR-SR because, in contrast to QLNМ-QQR, it also considers a sparse regularization

term. Algorithm 2 summarizes all of the steps involved in the proposed model.

Algorithm 2 The proposed QLNM-QQR-SR method for color image completion.

Input: The observed data $\dot{\mathbf{M}} \in \mathbb{H}^{M \times N}$ ($\mathcal{P}_{\Omega^c}(\dot{\mathbf{M}}) = \mathbf{0}$); ρ ; μ_{\max} ; β ; r .

- 1: **Initialize** $\tau = 0$; $\varepsilon > 0$; μ^0 ; $It_{\max} > 0$; $\dot{\mathbf{L}}^0 = eye(M, r)$; $\dot{\mathbf{R}}^0 = eye(r, N)$; $\dot{\mathbf{D}}^0 = eye(r, r)$; $\dot{\mathbf{X}}^0 = \dot{\mathbf{M}}$; $\dot{\mathbf{C}}^0 = \mathbf{0}$.
 - 2: **Repeat**
 - 3: **Step 1.** $\dot{\mathbf{L}}^{\tau+1}$, $\dot{\mathbf{R}}^{\tau+1}$: (39) and (40), respectively.
 - 4: **Step 2.** $\dot{\mathbf{D}}^{\tau+1}$: (44) and (45).
 - 5: **Step 3.** $\dot{\mathbf{X}}^{\tau+1} = \mathcal{P}_{\Omega}(\dot{\mathbf{M}}) + \mathcal{P}_{\Omega^c}(\frac{1}{2}(\dot{\mathbf{L}}^{\tau+1}\dot{\mathbf{D}}^{\tau+1}\dot{\mathbf{R}}^{\tau+1} - \frac{\dot{\mathbf{E}}^{\tau}}{\mu^{\tau}} + \mathcal{I}(\dot{\mathbf{C}}^{\tau} + \frac{\dot{\mathbf{E}}^{\tau}}{\mu^{\tau}})))$.
 - 6: **Step 4.** $\dot{\mathbf{C}}^{\tau+1} = S_{\frac{\mu^{\tau}}{\mu^{\tau}}}(\mathcal{T}(\dot{\mathbf{X}}^{\tau+1}) - \frac{\dot{\mathbf{E}}^{\tau}}{\mu^{\tau}})$.
 - 7: $\dot{\mathbf{E}}^{\tau+1} = \dot{\mathbf{E}}^{\tau} + \mu^{\tau}(\dot{\mathbf{X}}^{\tau+1} - \dot{\mathbf{L}}^{\tau+1}\dot{\mathbf{D}}^{\tau+1}\dot{\mathbf{R}}^{\tau+1})$.
 - 8: $\dot{\mathbf{F}}^{\tau+1} = \dot{\mathbf{F}}^{\tau} + \mu^{\tau}(\dot{\mathbf{C}}^{\tau+1} - \mathcal{T}(\dot{\mathbf{X}}^{\tau+1}))$.
 - 9: $\mu^{\tau+1} = \min(\rho\mu^{\tau}, \mu_{\max})$.
 - 10: **Until convergence**
- Output:** $\dot{\mathbf{L}}^{\tau+1}$, $\dot{\mathbf{D}}^{\tau+1}$, $\dot{\mathbf{R}}^{\tau+1}$, $\dot{\mathbf{X}}^{\tau+1}$, and $\dot{\mathbf{C}}^{\tau+1}$.
-

4.3. Complexity analysis

The computational complexities of our proposed three approaches are investigated in this subsection. According to Algorithm 1, the computation of the QQR decomposition of two quaternion matrices accounts for most of the computing cost of each iteration of QLNM-QQR. Additionally, these two quaternion matrices have sizes of $M \times r$ and $N \times r$, respectively, where $r < \min\{M, N\}$. As a result, the complexity is approximately $O(r^2(M + N) - r^3)$. Similarly, the complexity of IRQLNM-QQR is also around $O(r^2(M + N) - r^3)$. Regarding the algorithmic complexity of the QLNM-QQR-SR technique, the transformation operator $\mathcal{T}(\cdot)$ adds significant additional algorithmic complexity on top of the QQR decomposition computation. $\mathcal{T}(\cdot)$ corresponds to a complexity of approximately $O(M^2N^2 + MN)$. The proposed QLNM-QQR-SR approach's overall computing complexity is thus around $O(M^2N^2 + MN)$ per iteration.

However, methods directly based on the QNN, such as LRQA-G [16], need to calculate the QSVD of the quaternion matrix with size $M \times N$, and the complexity is about $O(\min(MN^2, M^2N))$. It is clear that the computational cost of QQR decomposition of two quaternion matrices of size $M \times r$ and $N \times r$ is smaller than that of QSVD of the quaternion matrix with size $M \times N$. Additionally, the computational complexity of each iteration for the LRQMC method is with an estimated cost of $O(\tilde{r}(\tilde{r}^2 + (M + N)\tilde{r} + MN))$, where \tilde{r} denotes the estimated rank of the complex representation matrix of $\dot{\mathbf{X}}$ of size $2M \times 2N$. The computational cost of IRLNM-QR is around $O(r^2(M + N))$. It can be found that both QLNM-QQR and IRQLNM-QQR approaches our proposed have computational complexities that are comparable to IRLNM-QR while being less than those of LRQA and LRQMC.

5. Simulation results and discussion

To show the effectiveness of the proposed three quaternion-based completion techniques (i.e., QLNМ-QQR, IRQLNM-QQR, and QLNМ-QQR-SR), we perform numerical experiments on natural color images and color medical images in this part. We also present corresponding numerical results analysis for the three quaternion-based completion methods. On a MATLAB 2019b platform with an i7-9700 CPU and 16 GB memory, we run all of the tests.

Evaluation metrics: Peak signal-to-noise ratio (PSNR) and structural similarity (SSIM) are two extensively used metrics that we utilize to assess the effectiveness of the proposed QQR-QNN-SR, IRQLNM-QQR, and QLNМ-QQR-SR. Better recovery performance is indicated by higher PSNR and SSIM.

We present the experimental results and analysis of the QLNМ-QQR, IRQLNM-QQR, and QLNМ-QQR-SR approaches. Specifically, we conduct numerical experiments on matrices with randomly missing entries, including those composed of quaternions. To showcase the effectiveness of our method, we consider the missing ratio (MR) of entries ranging from 50% to 85%.

Method comparison: Several popular completion techniques, namely, WNNM [2], MC-NC [37], IRLNM-QR [19], TNN-SR [26], QLNF [17], TQLNA [17], LRQA-G [16], and LRQMC [4] are contrasted with the proposed QLNМ-QQR, IRQLNM-QQR, and QLNМ-QQR-SR approaches. Whereas WNNM, MC-NC, IRLNM-QR, and TNN-SR are LRMC-based completion algorithms, QLNF, TQLNA, LRQA-G, and LRQMC are LRQMC-based completion methods. Like the processing in [26], the approaches based on real matrix completion handle the three color channels individually first before combining their output to produce the final product.

Experimental results on the eight natural color images: In our tests, eight frequently used 256×256 natural color images, as shown in Fig. 1, are chosen as the test images (four from McMaster Datase [38]). Our experiments used the following parameters for QLNМ-QQR: $\mu^0 = 0.003, \rho = 1.05$. And the value of r is set to 65, 90, 105, and 125, corresponding to MR values of 85%, 75%, 65%, and 50%, respectively. For IRQLNM-QQR, we set $\mu^0 = 0.003$ and $\rho = 1$. The value of r is set to 115, 125, 155, and 170, corresponding to MR values of 85%, 75%, 65%, and 50%, respectively. To implement IRLNM-QQR, we set the values of parameters ζ and V in (59) to 10 and 3, respectively. As for the QLNМ-QQR-SR method, μ^0, β , and ρ are set as 0.5, 0.5, and 1.05, respectively. The parameter r is assigned the values 60, 85, 100, and 120, which correspond to MR (missing rate) values of 85%, 75%, 65%, and 50%, respectively. As the value of MR increases, the number of missing pixels increases, and the corresponding rank decreases.

The recovery results for MR= 75% are compared among different methods, as shown in Fig. 2. The results of the quantitative evaluation for different methods under different missing ratios (MR) are presented in Table 1. To

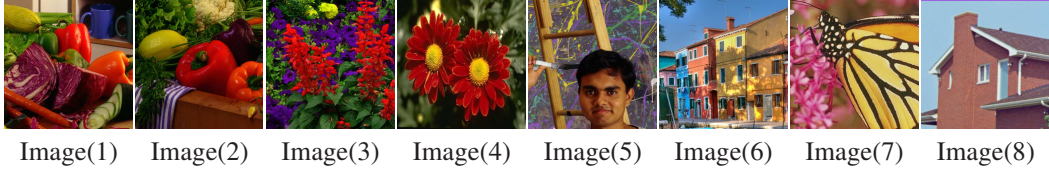


Fig. 1. Ground truth: Image(1)-Image(8) are eight color images, each with dimensions of $256 \times 256 \times 3$.

illustrate the superior performance of our proposed approaches, we present in Fig. 3 the visual results for image(2) and image(5) recovered using our approaches as well as several state-of-the-art approaches, all with a missing rate (MR) of 85%.

The results presented in Table 1 and Fig. 2 indicate that both QLNM-QQR and IRQLNM-QQR exhibit superior completion performance compared to WNNM. IRQLNM-QQR achieves superior completion results, higher PSNR and SSIM values compared to IRLNM-QR, and QLNM-QQR generally outperforms IRLNM-QR. Also, when MR is large, IRQLNM-QQR outperforms MC-NC. These results demonstrate the effectiveness of quaternion representations in solving color image completion problems. Based on Theorem 7, the IRQLNM-QQR method will approach the optimal solution of an LRQA-W minimization model. Additionally, as discussed in [16], LRQA-based models using non-convex functions demonstrate similar performance in the color image completion problem. Moreover, compared to LRQA-N and LRQA-L, the LRQA-G method has been found to have the best completion results. Table 1 indicates that the IRQLNM-QQR method can achieve numerical results comparable to LRQA-G. Furthermore, when the missing rate is high, the IRQLNM-QQR method generally outperforms the LRQA-G method. Also, the experimental results suggest that IRLNM-QQR exhibits superior precision to QLNM-QQR.

According to the results presented in Fig. 2 and Table 1, it can be observed that the QLNM-QQR-SR method proposed in this paper outperforms other methods in terms of both visual and quantitative assessments. The results indicate that incorporating sparse prior information is crucial for achieving better completion results, as both TNN-SR and QLNM-QQR-SR outperform other methods. Furthermore, QLNM-QQR-SR performs better than TNN-SR, which can be attributed to the ability of quaternions to characterize color images better. Based on the visual results presented in Fig. 3, our proposed method outperforms other state-of-the-art methods in terms of recovering more details from the observed images.

Experimental results on the color medical images: The continuous development of medical imaging equipment has revolutionized healthcare by providing accurate and detailed visual information about the human body. Magnetic resonance imaging (MRI) and positron emission tomography (PET) are widely used imaging techniques for capturing organs' structural and functional characteristics, respectively. Fusing these two types of data can greatly enhance the interpretation of tissue and organ behavior, thereby improving the accuracy of diagnoses. Therefore, the analysis of



Fig. 2. (a) Ground truth. From top to bottom: Image(1)-Image(8). (b) Observation (MR=75%). (c)-(m) are the restored results of WNNM, MC-NC, IRLNM-QR, TNN-SR, QLNF, TQLNA, LRQA-G, LRQMC, QLNM-QQR, IRQLNM-QQR, and QLNM-QQR-SR, respectively.

their overlay is of great importance in medical diagnosis. However, medical images may be incomplete for various reasons, such as equipment limitations or patient movements during examinations, which can negatively impact the accuracy of disease diagnosis. Quaternion completion-based models can be employed to address this issue.

Eight color medical images of size 256×256 , obtained from “The Whole Brain Atlas”¹ medical image database provided by Harvard Medical School, were used in the experiments. To leverage the information in the color medical images more effectively, we preprocessed the eight medical images by extracting sub-images with a size of 141×141 for subsequent experimental analysis. Fig. 4 shows the eight original medical images along with their corresponding sub-images obtained after preprocessing.

For the experiment conducted at an MR=85%, we used the same parameter settings for μ^0 , ρ , and β in the QLNM-QQR, IRQLNM-QQR, and QLNM-QQR-SR methods as in the previous experiment. The r values for QLNM-QQR, IRQLNM-QQR, and QLNM-QQR-SR were set to 55, 80, and 45, respectively. The IRLNM-QQR method was also implemented with the values of ζ and V set to 10 and 3, respectively, in (59). Fig. 5 displays the recovered color medical images using different methods for visual comparison. Fig. 5 visually demonstrates the superiority of our proposed QLNM-QQR-SR approach over all other methods. The numerical comparison of different methods in terms

¹<http://www.med.harvard.edu/AANLIB/home.html>



Fig. 3. The image recovery outcomes of $MR = 85\%$ on Image(2) and Image(5). (a) Ground truth. (b) Observation. (c)-(m) are the recovery outcomes of WNNM, MC-NC, IRLNM-QR, TNN-SR, QLNF, TQLNA, LRQA-G, LRQMC, QLNM-QQR, IRQLNM-QQR, and QLNM-QQR-SR, respectively.

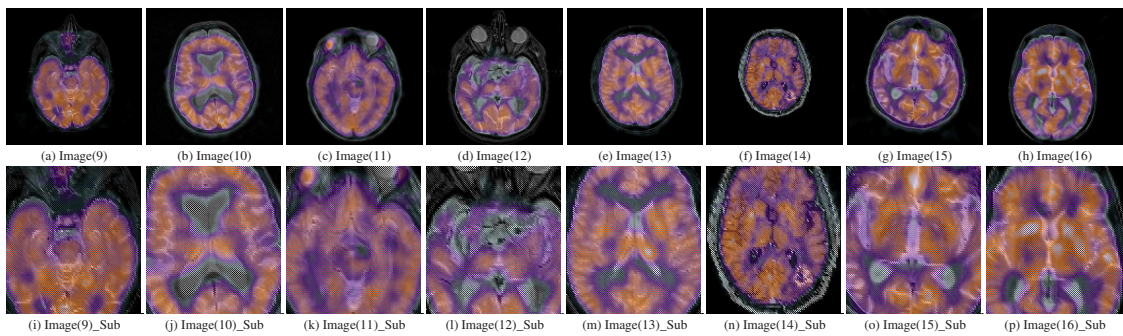


Fig. 4. (a)-(h) are the eight original color medical images with size $256 \times 256 \times 3$. (i)-(p) Ground truth: Image(9)_Sub-Image(16)_Sub are the corresponding sub-images with size $141 \times 141 \times 3$.

Table 1: A comparison of quantitative assessment indices (PSNR/SSIM) across different methods on the set of eight color images.

Methods:	WNNM	MC-NC	IRLNM-QR	TNN-SR	QLNF	TQLNA	LRQA-G	LRQMC	QLNM-QQR	IRQLNM-QQR	QLNM-QQR-SR
MR = 50%											
Images:											
Image(1)	23.386/0.848	26.939/0.935	24.336/0.888	28.657/0.955	24.223/0.862	27.020/0.909	26.561/0.927	27.007/0.936	26.208/0.923	26.557/0.930	29.156/0.959
Image(2)	24.837/0.861	28.233/0.937	25.767/0.899	30.070/0.957	25.312/0.872	28.260/0.921	27.748/0.928	28.319/0.938	27.442/0.926	27.771/0.930	30.487/0.960
Image(3)	19.995/0.759	23.562/0.878	22.155/0.841	25.357/0.918	21.659/0.814	23.927/0.878	23.376/0.873	23.306/0.877	23.057/0.869	23.603/0.881	25.767/0.924
Image(4)	24.231/0.877	27.586/0.950	25.085/0.899	29.205/0.965	25.007/0.853	27.497/0.918	27.267/0.944	27.499/0.950	26.904/0.940	27.223/0.945	29.507/0.967
Image(5)	22.795/0.731	26.294/0.862	24.214/0.811	28.030/0.903	23.840/0.749	26.411/0.826	25.985/0.850	26.448/0.865	25.693/0.846	26.097/0.859	28.681/0.915
Image(6)	22.246/0.883	25.686/0.943	22.802/0.898	27.046/0.958	22.352/0.884	25.734/0.941	25.266/0.937	25.658/0.942	24.790/0.931	25.081/0.936	27.417/0.961
Image(7)	21.406/0.877	24.439/0.938	21.018/0.886	27.303/0.968	20.249/0.861	24.358/0.933	23.969/0.931	24.319/0.937	23.433/0.926	23.406/0.926	27.933/0.971
Image(8)	27.822/0.920	29.482/0.956	26.564/0.925	33.175/0.978	26.448/0.913	30.684/0.959	29.925/0.957	30.434/0.962	29.493/0.954	29.284/0.954	33.635/0.980
Aver.	23.340	26.528	23.993	28.605	23.636	26.736	26.262	26.624	25.878	26.128	29.073
MR = 65%											
Images:											
Image(1)	20.815/0.771	24.155/0.884	22.029/0.834	26.489/0.931	22.677/0.823	24.292/0.859	23.823/0.874	24.103/0.886	23.323/0.866	23.841/0.878	26.996/0.938
Image(2)	22.196/0.784	25.546/0.889	23.600/0.848	27.936/0.932	23.867/0.831	25.613/0.871	25.180/0.879	25.652/0.892	24.644/0.873	25.233/0.882	28.422/0.937
Image(3)	17.533/0.738	20.605/0.777	20.154/0.758	23.277/0.870	20.153/0.743	21.465/0.798	20.907/0.786	21.249/0.806	20.521/0.776	21.193/0.801	23.752/0.883
Image(4)	21.791/0.786	24.960/0.900	22.829/0.844	27.225/0.944	23.498/0.814	24.980/0.858	24.668/0.892	24.783/0.901	24.114/0.883	24.670/0.896	27.611/0.950
Image(5)	20.130/0.607	23.535/0.763	22.181/0.719	25.765/0.844	22.342/0.669	23.759/0.728	23.405/0.754	23.609/0.770	22.957/0.743	23.620/0.769	26.385/0.862
Image(6)	19.226/0.791	22.618/0.891	20.442/0.835	24.415/0.925	20.705/0.836	22.532/0.884	22.154/0.878	21.797/0.872	21.540/0.865	22.122/0.880	24.854/0.932
Image(7)	18.091/0.776	21.101/0.877	18.901/0.834	24.607/0.943	18.651/0.813	21.090/0.874	20.749/0.871	20.333/0.868	20.123/0.861	20.501/0.870	25.185/0.948
Image(8)	24.594/0.866	27.095/0.923	24.384/0.883	30.836/0.963	25.028/0.879	27.380/0.917	26.893/0.917	26.272/0.914	26.237/0.909	26.525/0.917	31.369/0.967
Aver.	20.547	23.702	21.815	26.319	22.115	23.889	23.472	23.475	22.932	23.463	26.822
MR = 75%											
Images:											
Image(1)	18.794/0.689	21.882/0.818	20.580/0.788	25.004/0.907	21.574/0.784	22.470/0.810	22.024/0.822	21.788/0.826	21.269/0.806	22.072/0.830	25.455/0.914
Image(2)	19.965/0.704	23.122/0.825	22.028/0.801	26.621/0.909	22.547/0.787	23.565/0.815	23.189/0.825	22.931/0.828	22.537/0.816	23.297/0.830	27.090/0.917
Image(3)	15.707/0.529	18.252/0.652	18.884/0.683	21.926/0.822	19.082/0.678	19.815/0.719	19.287/0.701	19.290/0.708	18.870/0.684	19.577/0.719	22.431/0.842
Image(4)	19.676/0.689	22.652/0.831	21.256/0.795	25.811/0.926	22.054/0.772	22.977/0.800	22.731/0.836	22.207/0.835	21.962/0.820	22.694/0.842	26.234/0.937
Image(5)	18.105/0.495	21.118/0.646	20.654/0.637	24.263/0.789	21.185/0.600	21.800/0.630	21.398/0.653	21.153/0.657	20.848/0.637	21.703/0.674	24.798/0.812
Image(6)	16.971/0.689	19.952/0.812	18.926/0.776	22.889/0.895	19.517/0.791	20.480/0.823	20.153/0.816	20.074/0.817	19.389/0.793	20.183/0.820	23.342/0.906
Image(7)	15.317/0.652	17.749/0.778	17.387/0.787	22.758/0.918	17.411/0.768	18.731/0.810	18.528/0.810	18.697/0.821	17.850/0.794	18.480/0.814	23.406/0.928
Image(8)	21.725/0.769	24.816/0.881	22.782/0.843	28.964/0.946	23.637/0.844	24.673/0.866	24.580/0.873	23.961/0.868	23.839/0.860	24.386/0.875	29.373/0.951
Aver.	18.283	21.193	20.312	24.780	20.876	21.814	21.486	21.263	20.821	21.549	25.266
MR = 85%											
Images:											
Image(1)	16.018/0.562	17.777/0.644	18.637/0.713	23.413/0.871	19.658/0.713	19.949/0.726	19.720/0.738	19.042/0.731	18.771/0.710	19.758/0.748	23.836/0.883
Image(2)	17.665/0.603	19.079/0.684	19.914/0.727	24.561/0.866	20.541/0.711	21.201/0.737	20.895/0.747	20.059/0.743	19.784/0.725	20.901/0.750	25.064/0.878
Image(3)	13.367/0.377	15.852/0.485	17.084/0.560	20.328/0.754	17.103/0.549	17.801/0.598	17.361/0.577	17.320/0.578	16.890/0.546	17.583/0.596	20.768/0.779
Image(4)	17.216/0.569	18.991/0.682	19.428/0.719	24.307/0.896	20.149/0.699	20.550/0.711	20.520/0.749	19.889/0.751	19.572/0.725	20.461/0.757	24.744/0.910
Image(5)	15.578/0.349	17.502/0.438	18.862/0.519	22.712/0.708	19.465/0.490	19.703/0.502	19.399/0.531	18.945/0.527	18.587/0.503	19.683/0.551	23.152/0.734
Image(6)	14.105/0.523	15.674/0.599	16.885/0.672	20.992/0.842	17.322/0.685	17.635/0.703	17.687/0.710	17.711/0.713	16.929/0.674	17.772/0.718	21.384/0.858
Image(7)	12.230/0.471	14.049/0.593	15.408/0.705	20.556/0.874	14.970/0.653	15.751/0.690	16.034/0.714	15.744/0.721	15.507/0.699	16.055/0.723	21.184/0.889
Image(8)	18.320/0.628	20.356/0.738	19.730/0.730	26.484/0.916	21.107/0.762	21.554/0.776	21.573/0.788	21.586/0.798	20.655/0.760	21.603/0.797	26.825/0.922
Aver.	15.562	17.410	18.244	22.919	18.789	19.268	19.149	18.787	18.337	19.227	23.370

of PSNR and SSIM values for recovered medical images at MR=85% is shown in Table 2. The results show that the IRQLNM-QQR method is superior to the QLNM-QQR and LRQA-G methods regarding numerical and visual results. It is challenging to improve the quality of recovered images at this level of MR. However, our proposed QLNM-QQR-SR method outperforms other methods in terms of PSNR and SSIM values, as demonstrated by Table 2.

6. Conclusions

In this study, we created a novel method called QLNM-QQR for completing color images using the tool of quaternion representation of color images. The method is based on the quaternion $L_{2,1}$ -norm and a Tri-Factorization of a quaternion matrix called CQSVD-QQR. The coupling between color channels can be naturally handled with this approach and representing color pixels as vector units rather than scalars in the quaternion representation results in better retention of color information. The method avoids the need to calculate the QSVD of large quaternion matrices, which reduces the computational complexity compared to traditional LRQMC methods. According to theoretical analysis, the quaternion $L_{2,1}$ -norm of a submatrix in QLNM-QQR is capable of converging to its QNN. To enhance

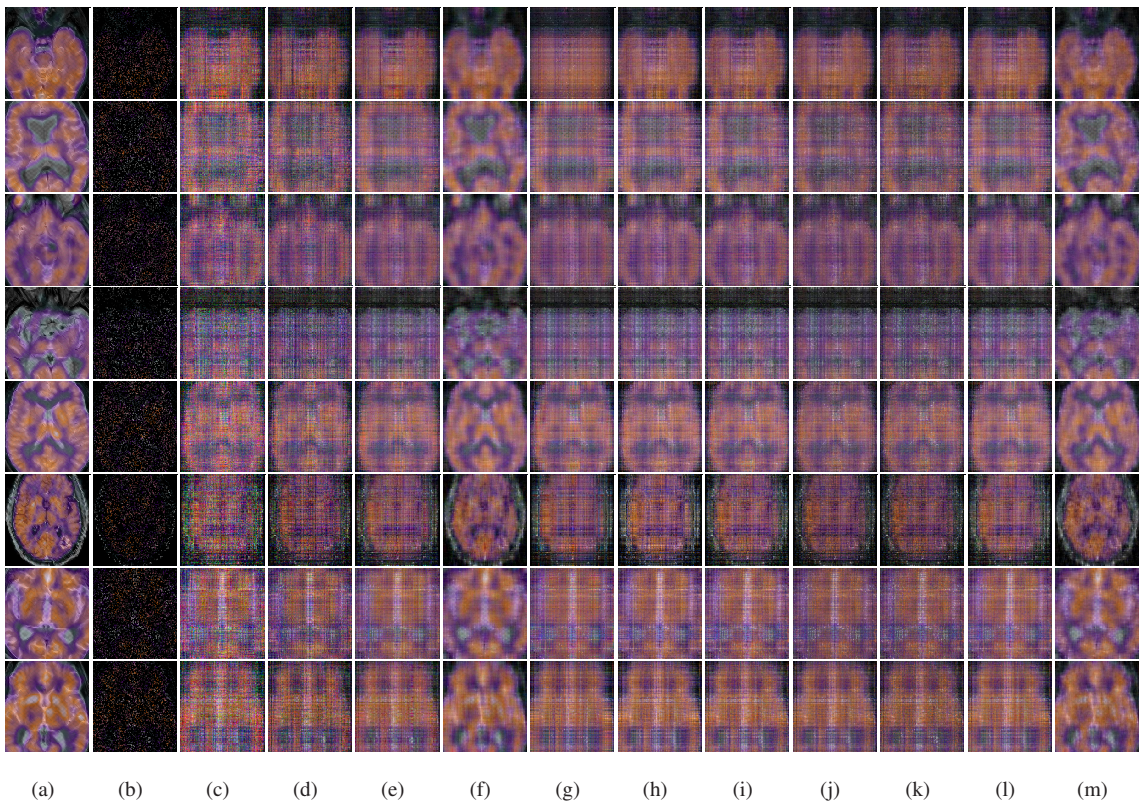


Fig. 5. (a) Ground truth. From top to bottom: Image(9)_Sub-Image(16)_Sub. (b) Observation (MR=75%). (c)-(m) are the restored results of WNNM, MC-NC, IRLNM-QR, TNN-SR, QLNF, TQLNA, LRQA-G, LRQMC, QLNM-QQR, IRQLNM-QQR, and QLNM-QQR-SR, respectively.

Table 2: A comparison of quantitative assessment indices (PSNR/SSIM) across different methods on the set of eight color medical images.

Methods:	WNNM	MC-NC	IRLNM-QR	TNN-SR	QLNF	TQLNA	LRQA-G	LRQMC	QLNM-QQR	IRQLNM-QQR	QLNM-QQR-SR
Images:	MR = 85%										
Image(9)_Sub	14.693/0.432	16.221/0.494	17.768/0.588	21.499/0.774	17.462/0.538	18.169/0.588	18.026/0.589	18.418/0.611	17.311/0.550	18.188/0.613	21.729/0.781
Image(10)_Sub	13.239/0.447	14.673/0.501	16.528/0.627	21.003/0.838	16.470/0.600	16.905/0.635	16.637/0.624	15.985/0.590	15.712/0.568	16.848/0.641	21.494/0.854
Image(11)_Sub	14.949/0.480	16.422/0.543	17.675/0.637	22.786/0.860	17.476/0.605	18.336/0.661	18.116/0.645	17.639/0.621	17.366/0.598	18.191/0.667	23.031/0.870
Image(12)_Sub	12.798/0.436	14.124/0.476	15.855/0.612	18.968/0.783	16.053/0.613	15.949/0.614	15.880/0.604	16.119/0.611	15.499/0.567	16.039/0.628	19.073/0.787
Image(13)_Sub	13.445/0.415	15.158/0.495	16.171/0.576	21.103/0.830	16.836/0.595	17.166/0.623	16.883/0.605	16.541/0.590	16.144/0.555	17.003/0.627	21.437/0.843
Image(14)_Sub	10.679/0.258	12.762/0.321	13.536/0.407	16.670/0.597	14.028/0.399	13.577/0.391	13.993/0.406	14.108/0.401	13.827/0.374	13.997/0.431	16.844/0.611
Image(15)_Sub	12.684/0.468	14.198/0.527	15.830/0.640	20.442/0.861	15.531/0.617	16.031/0.652	15.858/0.635	15.541/0.614	15.265/0.585	15.986/0.656	20.726/0.873
Image(16)_Sub	12.481/0.420	13.977/0.466	15.403/0.576	20.481/0.829	15.772/0.591	16.138/0.620	15.990/0.604	16.329/0.622	15.285/0.546	16.123/0.625	20.933/0.843
Aver.	14.949	16.422	17.768	22.786	17.476	18.336	18.116	18.418	17.366	18.191	23.031

its performance, we introduce an improved version called IRQLNM-QQR that uses iteratively reweighted quaternion $L_{2,1}$ -norm minimization. According to theoretical analysis, IRQLNM-QQR is equally precise as an LRQA-W minimization method. Additionally, we incorporate sparse regularization into the QLNM-QQR method to develop QLNM-QQR-SR. The experimental results obtained from both natural color images and color medical images indicate that IRLNM-QQR achieves almost comparable accuracy to the LRQA-G method and outperforms QLNM-QQR in precision. The experimental results also demonstrate that the QLNM-QQR-SR method proposed in this research displays better performance in both numerical accuracy and visual quality compared to several state-of-the-art techniques. Besides, we have proven that the quaternion $L_{2,1}$ -norm is an upper bound for the quaternion nuclear norm of a quaternion matrix. As a result, the proposed methods have broad applicability and can enhance the performance of a variety of techniques, including multiview data analysis, quaternion matrix/tensor completion, and low-rank representation based on quaternion nuclear norm.

Acknowledgments

This work was supported by University of Macau (MYRG2019-00039-FST), Science and Technology Development Fund, Macao S.A.R (FDCT/0036/2021/AGJ), and Science and Technology Planning Project of Guangzhou City, China (Grant No. 201907010043).

Declaration of competing interest

The authors declare that they have no known competing financial interests or personal relationships that could have appeared to influence the work reported in this paper.

Appendix A. Proof of Theorem 5

Proof. The quaternion $L_{2,1}$ -norm of $\dot{\mathbf{X}}$ can be rewritten as follows:

$$\|\dot{\mathbf{X}}\|_{2,1} = \sum_{n=1}^N \sqrt{\sum_{m=1}^M |\dot{\mathbf{X}}_{mn}|^2} = \sum_{n=1}^N \|\dot{\mathbf{X}}_{\cdot n}\|_2, \quad (\text{A.1})$$

where $\|\dot{\mathbf{X}}_{\cdot n}\|_2 = \sqrt{\sum_{m=1}^M |\dot{\mathbf{X}}_{mn}|^2}$. Since two of the terms in (42) are convex, there is only one optimal solution. With the use of the associated theories for quaternion matrix derivatives in [39], we get

$$\begin{aligned} \frac{\partial \mathcal{J}(\dot{\mathbf{X}}_{\cdot n})}{\partial \dot{\mathbf{X}}_{\cdot n}} &= \beta \frac{\partial \|\dot{\mathbf{X}}_{\cdot n}\|_2}{\partial \dot{\mathbf{X}}_{\cdot n}} + \frac{1}{2} \frac{\partial \text{Tr}[(\dot{\mathbf{X}}_{\cdot n} - \dot{\mathbf{Y}}_{\cdot n})^H (\dot{\mathbf{X}}_{\cdot n} - \dot{\mathbf{Y}}_{\cdot n})]}{\partial \dot{\mathbf{X}}_{\cdot n}} \\ &= \beta \frac{\dot{\mathbf{X}}_{\cdot n}}{\|\dot{\mathbf{X}}_{\cdot n}\|_2} + \frac{1}{4} (\dot{\mathbf{X}}_{\cdot n} - \dot{\mathbf{Y}}_{\cdot n}) \\ &= \beta \frac{\dot{\mathbf{Y}}_{\cdot n}}{\|\dot{\mathbf{Y}}_{\cdot n}\|_2} + \frac{1}{4} (\dot{\mathbf{X}}_{\cdot n} - \dot{\mathbf{Y}}_{\cdot n}) (\|\dot{\mathbf{Y}}_{\cdot n}\|_2 > 4\beta). \end{aligned} \quad (\text{A.2})$$

We can find the unique solution to problem (42) by setting (A.2) to zero as follows:

$$\begin{aligned} \tilde{\dot{\mathbf{X}}}_{\cdot n} &= \dot{\mathbf{Y}}_{\cdot n} - 4\beta \frac{\dot{\mathbf{Y}}_{\cdot n}}{\|\dot{\mathbf{Y}}_{\cdot n}\|_2} (\|\dot{\mathbf{Y}}_{\cdot n}\|_2 > 4\beta) \\ &= \frac{\dot{\mathbf{Y}}_{\cdot n}}{\|\dot{\mathbf{Y}}_{\cdot n}\|_2} (\|\dot{\mathbf{Y}}_{\cdot n}\|_2 - 4\beta) (\|\dot{\mathbf{Y}}_{\cdot n}\|_2 > 4\beta) \\ &= \frac{(\|\dot{\mathbf{Y}}_{\cdot n}\|_2 - 4\beta)_+}{\|\dot{\mathbf{Y}}_{\cdot n}\|_2} \dot{\mathbf{Y}}_{\cdot n}, \end{aligned} \quad (\text{A.3})$$

where $(y)_+ = \max\{y, 0\}$. □

Appendix B. Proof of Theorem 6

Proof. In line with (50), the optimal solution $\dot{\mathbf{X}}_{\text{opt}}^m$ of the problem in (55) is given by

$$\dot{\mathbf{X}}_{\text{opt}}^m = \min_{\dot{\mathbf{X}}^m} \frac{\omega_m}{\mu} \|\dot{\mathbf{X}}^m\|_* + \frac{1}{2} \|\dot{\mathbf{X}}^m - \dot{\mathbf{Y}}^m\|_F^2, \quad (m = 1, \dots, M) \quad (\text{B.1})$$

where $\dot{\mathbf{X}}_{\text{opt}} = \sum_{m=1}^M \dot{\mathbf{X}}_{\text{opt}}^m$. Assume that $\dot{\mathbf{Y}}^m = \dot{\mathbf{U}} \dot{\mathbf{\Sigma}} \dot{\mathbf{V}}^H$ is the QSVD of $\dot{\mathbf{Y}}^m$. We represent $\dot{\mathbf{U}}$ and $\dot{\mathbf{V}}$ as two partitioned matrices: $\dot{\mathbf{U}} = [\dot{\mathbf{u}}_1, \dots, \dot{\mathbf{u}}_M]$, and $\dot{\mathbf{V}} = [\dot{\mathbf{v}}_1, \dots, \dot{\mathbf{v}}_M]$, where $\dot{\mathbf{u}}_m$ and $\dot{\mathbf{v}}_m \in \mathbb{H}^M$ ($m = 1, \dots, M$). Based on Lemma 1, we

can give the closed-form solution of (B.1) as follows:

$$\begin{aligned}
\dot{\mathbf{X}}_{\text{opt}}^m &= \dot{\mathbf{U}} S_{\frac{\omega_m}{\mu}}(\Sigma) \dot{\mathbf{V}}^H \\
&= (\|\dot{\mathbf{Y}}^m\|_F - \frac{\omega_m}{\mu})_+ \dot{\mathbf{u}}_1 \dot{\mathbf{v}}_1^H \\
&= \frac{(\|\dot{\mathbf{Y}}^m\|_F - \frac{\omega_m}{\mu})_+}{\|\dot{\mathbf{Y}}^m\|_F} \dot{\mathbf{Y}}^m,
\end{aligned} \tag{B.2}$$

where $\|\dot{\mathbf{Y}}^m\|_F = \sigma_m$ is the only singular value of $\dot{\mathbf{Y}}^m$. Based on the above discusses, the optimal solution $\dot{\mathbf{X}}_{\text{opt}}$ is given by

$$\dot{\mathbf{X}}_{\text{opt}} = \dot{\mathbf{Y}} \mathbf{A}, \tag{B.3}$$

where $\mathbf{A} = \text{diag}(a_1, \dots, a_M)$, and

$$a_m = \frac{(\sigma_m - \frac{\omega_m}{\mu})_+}{\sigma_m}, \quad (m = 1, \dots, M) \tag{B.4}$$

□

Appendix C. Proof of Theorem 7

Proof. The IRQLNM-QQR algorithm produces a sequence of quaternion matrices $\{\dot{\mathbf{D}}^r\}$ that can converge to a diagonal matrix $\dot{\mathbf{D}}$ satisfying (49). As a result, the $\dot{\mathbf{D}}$ in (53) also converge to a diagonal matrix $\dot{\mathbf{T}}$. Therefore, we can reformulate the problem in (53) as follows:

$$\min_{\dot{\mathbf{D}}} \sum_{l=1}^r \partial g(\|\dot{\mathbf{D}}^l\|_*) \|\dot{\mathbf{D}}^l\|_* + \frac{\mu^r}{2} \|\dot{\mathbf{D}} - \dot{\mathbf{T}}\|_F^2, \tag{C.1}$$

Because $\|\dot{\mathbf{D}}^l\|_* = \sigma_l(\dot{\mathbf{D}})$, we can rewrite the above problem as follows:

$$\min_{\dot{\mathbf{D}}} \sum_{l=1}^r \partial g(\|\dot{\mathbf{D}}^l\|_*) \sigma_l(\dot{\mathbf{D}}) + \frac{\mu^r}{2} \|\dot{\mathbf{D}} - \dot{\mathbf{T}}\|_F^2. \tag{C.2}$$

Therefore, based on Lemma 2, we can solve the problem (C.2). □

References

- [1] Q. Liu, Z. Lai, Z. Zhou, F. Kuang, Z. Jin, A truncated nuclear norm regularization method based on weighted residual error for matrix completion, IEEE Trans. Image Process. 25 (1) (2015) 316–330.
- [2] S. Gu, Q. Xie, D. Meng, W. Zuo, X. Feng, L. Zhang, Weighted nuclear norm minimization and its applications to low level vision, Int. J. Comput. Vis. 121 (2) (2017) 183–208.
- [3] M. Yang, Y. Li, J. Wang, Feature and nuclear norm minimization for matrix completion, IEEE Trans. Knowl. Data Eng. 34 (5) (2020) 2190–2199.

- [4] J. Miao, K. I. Kou, Color image recovery using low-rank quaternion matrix completion algorithm, *IEEE Trans. Image Process.* 31 (2021) 190–201.
- [5] E. J. Candès, B. Recht, Exact matrix completion via convex optimization, *Found. Comput. Math.* 9 (2009) 717–772.
- [6] Y. Hu, D. Zhang, J. Ye, X. Li, X. He, Fast and accurate matrix completion via truncated nuclear norm regularization, *IEEE Trans. Pattern Anal. Mach. Intell.* 35 (9) (2012) 2117–2130.
- [7] S. Gu, L. Zhang, W. Zuo, X. Feng, Weighted nuclear norm minimization with application to image denoising, in: *Proceedings of the IEEE conference on computer vision and pattern recognition*, 2014, pp. 2862–2869.
- [8] Y. Xie, S. Gu, Y. Liu, W. Zuo, W. Zhang, L. Zhang, Weighted Schatten p -norm minimization for image denoising and background subtraction, *IEEE Trans. Knowl. Data Eng.* 25 (10) (2016) 4842–4857.
- [9] Z. Kang, C. Peng, J. Cheng, Q. Cheng, Logdet rank minimization with application to subspace clustering, *Comput. Intell. Neurosci.* 2015 (2015) 68–68.
- [10] Z. Wen, W. Yin, Y. Zhang, Solving a low-rank factorization model for matrix completion by a nonlinear successive over-relaxation algorithm, *Math. Program. Comput.* 4 (4) (2012) 333–361.
- [11] F. Shang, J. Cheng, Y. Liu, Z.-Q. Luo, Z. Lin, Bilinear factor matrix norm minimization for robust pca: Algorithms and applications, *IEEE Trans. Pattern Anal. Mach. Intell.* 40 (9) (2017) 2066–2080.
- [12] J. Han, K. I. Kou, J. Miao, Quaternion-based dynamic mode decomposition for background modeling in color videos, *Comput. Vis. Image Underst.* 224 (2022) 103560.
- [13] Y. Yu, Y. Zhang, S. Yuan, Quaternion-based weighted nuclear norm minimization for color image denoising, *Neurocomputing* 332 (2019) 283–297.
- [14] X.-X. Hu, K. I. Kou, Phase-based edge detection algorithms, *Math. Meth. Appl. Sci.* 41 (11) (2018) 4148–4169.
- [15] C. Zou, K. I. Kou, Y. Wang, Quaternion collaborative and sparse representation with application to color face recognition, *IEEE Trans. Image Process.* 25 (7) (2016) 3287–3302.
- [16] Y. Chen, X. Xiao, Y. Zhou, Low-rank quaternion approximation for color image processing, *IEEE Trans. Image Process.* 29 (2019) 1426–1439.
- [17] L. Yang, J. Miao, K. I. Kou, Quaternion-based color image completion via logarithmic approximation, *Inf. Sci.* 588 (2022) 82–105.
- [18] J. Miao, K. I. Kou, Quaternion-based bilinear factor matrix norm minimization for color image inpainting, *IEEE Trans. Signal Process.* 68 (2020) 5617–5631.
- [19] Q. Liu, F. Davoine, J. Yang, Y. Cui, Z. Jin, F. Han, A fast and accurate matrix completion method based on qr decomposition and $L_{2,1}$ -norm minimization, *IEEE Trans. Neural Netw. Learn. Syst.* 30 (3) (2018) 803–817.
- [20] J. Han, L. Yang, K. I. Kou, J. Miao, L. Liu, Low rank quaternion matrix completion based on quaternion qr decomposition and sparse regularizer, *arXiv preprint arXiv:2211.12793* (2022).
- [21] C. Hou, F. Nie, X. Li, D. Yi, Y. Wu, Joint embedding learning and sparse regression: A framework for unsupervised feature selection, *IEEE T. Cybern.* 44 (6) (2013) 793–804.
- [22] K. Tang, R. Liu, Z. Su, J. Zhang, Structure-constrained low-rank representation, *IEEE Trans. Neural Netw. Learn. Syst.* 25 (12) (2014) 2167–2179.
- [23] S. Xiao, M. Tan, D. Xu, Z. Y. Dong, Robust kernel low-rank representation, *IEEE Trans. Neural Netw. Learn. Syst.* 27 (11) (2015) 2268–2281.
- [24] F. Nie, J. Yuan, H. Huang, Optimal mean robust principal component analysis, in: *International conference on machine learning*, PMLR, 2014, pp. 1062–1070.
- [25] J. Yang, J. Wright, T. S. Huang, Y. Ma, Image super-resolution via sparse representation, *IEEE Trans. Image Process.* 19 (11) (2010) 2861–

2873.

- [26] J. Dong, Z. Xue, J. Guan, Z.-F. Han, W. Wang, Low rank matrix completion using truncated nuclear norm and sparse regularizer, *Signal Process.-Image Commun.* 68 (2018) 76–87.
- [27] L. Yang, Y. Liu, K. I. Kou, Quaternion optimized model with sparse regularization for color image recovery, arXiv preprint arXiv:2204.08629 (2022).
- [28] L. Zhang, L. Song, B. Du, Y. Zhang, Nonlocal low-rank tensor completion for visual data, *IEEE T. Cybern.* 51 (2) (2019) 673–685.
- [29] J. Fan, T. W. Chow, Matrix completion by least-square, low-rank, and sparse self-representations, *Pattern Recognit.* 71 (2017) 290–305.
- [30] L. Rodman, *Topics in quaternion linear algebra*, Princeton University Press, 2014.
- [31] W. R. Hamilton, Ii. on quaternions; or on a new system of imaginaries in algebra, *The London, Edinburgh, and Dublin Philosophical Magazine and Journal of Science* 25 (163) (1844) 10–13.
- [32] R. D. Schafer, On the algebras formed by the cayley-dickson process, *American Journal of Mathematics* 76 (2) (1954) 435–446.
- [33] F. Zhang, Quaternions and matrices of quaternions, *Linear Alg. Appl.* 251 (1997) 21–57.
- [34] M. Wei, Y. Li, F. Zhang, J. Zhao, *Quaternion Matrix Computations*, Nova Science Publisher, 2018.
- [35] W. Feng, B. Hu, Quaternion discrete cosine transform and its application in color template matching, in: *2008 Congress on Image and Signal Processing*, Vol. 2, IEEE, 2008, pp. 252–256.
- [36] M. Bahri, E. S. Hitzer, A. Hayashi, R. Ashino, An uncertainty principle for quaternion fourier transform, *Comput. Math. Appl.* 56 (9) (2008) 2398–2410.
- [37] F. Nie, Z. Hu, X. Li, Matrix completion based on non-convex low-rank approximation, *IEEE Trans. Image Process.* 28 (5) (2018) 2378–2388.
- [38] L. Zhang, X. Wu, A. Buades, X. Li, Color demosaicking by local directional interpolation and nonlocal adaptive thresholding, *J. Electron. Imaging* 20 (2) (2011) 023016–023016.
- [39] D. Xu, D. P. Mandic, The theory of quaternion matrix derivatives, *IEEE Trans. Signal Process.* 63 (6) (2015) 1543–1556.